

Sources and Radiations of the Fermi Bubbles

VLADIMIR A. DOGIEL^{1,*} AND CHUNG-MING KO^{2,†}

¹*I. E. Tamm Theoretical Physics Division of P. N. Lebedev Institute of Physics,
Leninskii pr. 53, 119991 Moscow, Russia*

²*Institute of Astronomy, Department of Physics and Center for Complex Systems,
National Central University, Zhongli Dist., Taoyuan City 320317, Taiwan (R.O.C.)*

ABSTRACT

Two enigmatic gamma-ray features in the Galactic central region, known as Fermi Bubbles (FBs), were found from Fermi-LAT data. An energy release (e.g., by tidal disruption events in the Galactic center, GC), generates a cavity with a shock that expands into the local ambient medium of the Galactic halo. A decade or so ago, a phenomenological model of the FBs was suggested as a result of routine star disruptions by the supermassive black hole in the GC which might provide enough energy for large-scale structures, like the FBs. In 2020, analytical and numerical models of the FBs as a process of routine tidal disruption of stars near the GC were developed, which can provide enough cumulative energy to form and maintain large scale structures like the FBs. The disruption events are expected to be $10^{-4} \sim 10^{-5} \text{ yr}^{-1}$, providing the average power of energy release from the GC into the halo of $\dot{E} \sim 3 \times 10^{41} \text{ erg s}^{-1}$, which is needed to support the FBs. Analysis of the evolution of superbubbles in exponentially stratified disks concluded that the FB envelope would be destroyed by the Rayleigh-Taylor (RT) instabilities at late stages. The shell is composed of a swept-up gas of the bubble, whose thickness is much thinner in comparison to the size of the envelope. We assume that hydrodynamic turbulence is excited in the FB envelope by the RT instability. In this case, the universal energy spectrum of turbulence may be developed in the inertial range of wavenumbers of fluctuations (the Kolmogorov-Obukhov spectrum). From our model we suppose the power of the FBs is transformed partly into the energy of hydrodynamic turbulence in the envelope. If so, hydrodynamic turbulence may generate MHD-fluctuations, which accelerate cosmic rays there and generate gamma-ray and radio emission from the FBs. We hope that this model may interpret the observed nonthermal emission from the bubbles.

Keywords: Galactic Center – Fermi Bubbles – central black hole – star disruptions – MHD turbulence – cosmic rays

1. INTRODUCTION: SOURCES OF THE FERMI BUBBLES

In this article we present our interpretation of the origin of the Fermi Bubbles (FBs). The discussion includes the energy release in the Galactic Center (GC) to the hydrodynamic envelope in Galactic halo, the excitation of MHD-turbulence that accelerates cosmic rays (CRs) in the halo, the processes of nonthermal emissions which are observed in X-ray, gamma-ray and radio ranges, and the high energy CRs escaping from the FBs to the Galactic disk. We present a puzzle of the FB picture, where many fragments are still missing in the mosaic. Many of them are interpreted but not completely understood yet. The goal of the article is to find a way for a proper solution to this problem.

The origin of the energy release in the FBs in GC is still an open question. This kiloparsec-scale structure was interpreted as a manifestation of past activity of the central supermassive black hole (SMBH) Sgr A* in the GC. The reader is referred to Figure 3 of [Predehl et al. \(2020\)](#), which shows the morphology of the gamma-ray bubbles (from Fermi) and the X-ray bubbles (from eROSITA). Observations in the GC showed structures above and below it in gamma-rays, microwave and X-rays. The eROSITA ([Predehl et al. 2020](#)) found giant bubbles in the X-ray range $0.1 \sim 2.4 \text{ keV}$ extending approximately 14 kiloparsecs above and below the GC. The estimated energy of the bubbles is around 10^{56} erg . The total luminosity in X-rays is about $10^{39} \text{ erg s}^{-1}$ which could be the result of past activities in the GC. The temperature of the envelope is about 0.3 keV , the velocity of the shock is about 340 km s^{-1} or of Mach number ≈ 1.5 , and the energy-release rate of the gas envelope is roughly $10^{41} \sim 10^{42} \text{ erg s}^{-1}$.

* dogiel@td.lpi.ru

† cmko@astro.ncu.edu.tw

The inner radius of the X-rays shell (about 7 kpc) coincides spatially with the region of GeV gamma-rays in the range $1 \sim 100$ GeV with the luminosity of $F_\gamma \approx 4 \times 10^{37}$ erg s^{-1} (Su et al. 2010). The bubble structure in the GC was also revealed in the range of microwaves which coincides nicely with that of gamma-rays (Planck Collaboration 2013). The flux is in the range $23 \sim 61$ GHz, and the luminosity is $\Phi_\nu \approx 1 \sim 5 \times 10^{36}$ erg s^{-1} .

Similar giant structures near the GC were found earlier in the radio in hundred MHz (the North Polar Spur, see Sofue 1977) and in 1.5 keV X-ray emission (see Bland-Hawthorn & Cohen 2003). These structures were postulated as bipolar supershells which were produced by starbursts. A shock front was supposed to reach a radius 10 kpc in the polar regions which could be consistent with the GC explosions. This model required an energy release of about 10^{55} erg at the GC, and periodic activity on a timescale of $10 \sim 15$ Myr.

Mou et al. (2023) suggested that the nature of North Polar Spur in the GC agreed with the eROSITA bubble of ages about 20 Myr (Predehl et al. 2020).

Bubbles were also discovered in other galaxies (see review by Sarkar 2024). Fig. 1 shows superbubbles from the galaxy NGC 3079.



Figure 1. Two superbubbles in the galaxy NGC 3079 observed in X-ray (purple and pink). Image obtained from <https://chandra.harvard.edu/photo/2019/ngc3079>. Image credit: X-ray: NASA/CXC/University of Michigan/J-T Li et al.; Optical: NASA/STScI.

The total energy needed to generate large Galactic outflows is assumed to be in the range up to about 10^{56} erg. This energy release in the GC may be compelling evidence for a huge energetic explosion occurred in the GC a few ($2 \sim 8$) million years ago, (see, e.g., Bland-Hawthorn & Cohen 2003, and references therein). For examples, Nayakshin & Zubovas (2018) assumed a capture of a giant molecular cloud of mass $\sim 10^5 M_\odot$ in the GC about one Myr ago; and Yang et al. (2012, 2022) suggested a model of FBs as a results of the past activity at the GC.

Alternative models of the bubbles were suggested by, e.g., Cheng et al. (2006, 2007, 2011), Mertsch & Sarkar (2011), Zubovas & Nayakshin (2012), Ko et al. (2020),

etc. They suggested that the source of energy of the bubbles is sporadic energy releases in the GC by stellar tidal disruption events (TDEs) near the central SMBH (see also other suggestions such as active star-formation near the GC, e.g., Zhang et al. 2024). The motion of nearby stars orbiting around Sgr A* (the GC) has been observed more than two decades (Ghez et al. 2005; Gillessen et al. 2009; Genzel et al. 2010). Analysis of the motions gave an estimated mass of about $4.4 \times 10^6 M_\odot$ for the central SMBH. For an illustration of orbits of stars around Sgr A*, see Figure 16 of Gillessen et al. (2009). For the motion of stars orbiting Sgr A*, the reader is referred to <https://www.eso.org/public/videos/eso1825e> (or <https://www.youtube.com/watch?v=TF8THY5spmo>); and for animation of stellar orbits around Sgr A* to <https://www.eso.org/public/videos/eso1825f> (or <https://www.youtube.com/watch?v=wuyuj7-XE8RE>), <https://www.youtube.com/watch?v=tMax0KgyZZU>.

TDE occurs when a star is getting too close to a SMBH (closer than the tidal radius). The classic picture is the star is disrupted by the tidal force, and after half of the stellar debris is in unbound orbits and the other half in bound orbits and fallback towards black hole (Ree 1988). The problem is how and how much energy is released into the host galaxy. For instance, how much energy is carried away by the unbound debris, and how much binding energy is released by the bound debris, say through accretion. Theoretically, it is possible to have 5% of the rest mass energy of the star being released (for a solar type star it is about 10^{53} erg). However, the results from observations are mixed, from several 10^{51} to 10^{53} erg. It is an active area of research to study TDE from different perspectives (to name a few, e.g., Burrows et al. 2011; Zauderer et al. 2011; Donato et al. 2014; Piran et al. 2015; Metzger & Stone 2016; Kara et al. 2016; Lin et al. 2017; Dai et al. 2018; Lu & Kumar 2018; Mockler & Ramirez-Ruiz 2021; Goodwin et al. 2023). The reader is also referred to reviews like Dai et al. (2021) and Gezari (2021). Another issue is the rate of TDEs at the centre of a galaxy with a SMBH. It is conceivable that the rate depends on the type of galaxy and the environment near the black hole. A typical estimation is roughly $10^{-4} \sim 10^{-5}$ yr^{-1} (e.g., Stone & Metzger 2016; Hung et al. 2018; Sarkar et al. 2023).

Ko et al. (2020) adopted the TDE model of Dai et al. (2018) and obtained the outflow energy of an event is about $10^{52} \sim 10^{53}$ erg (the outflow velocity is about $0.1 \sim 0.3$ the speed of light). Together with an event rate about 10^{-4} yr^{-1} will provide an average power about $\dot{E} \sim 3 \times 10^{41}$ erg s^{-1} , which will be sufficient to power the FBs. Miller & Bregman (2016) inferred a bubble expansion rate of 490 $km s^{-1}$, an age of 4.3 Myr, and a luminosity 2.3×10^{42} erg s^{-1} (see also the review of FBs in Sarkar 2024).

Recently, evidence of the energy release at Sgr A* was interpreted as the result of the latest stellar disruption. Two elongated chimneys of about 150 pc near the GC were found in the X-ray (Ponti et al. 2019, 2021) and radio (Heywood et al. 2019) ranges. In both cases the total energy of the chimneys was estimated to be about 10^{53} erg or below, which might be a result of the latest TDE by the central SMBH.

Similar processes of stellar disruption at the galactic center of other galaxies were observed. For example, X-ray transient Swift J164449.3+573451 (also known as GRB 110328A) was detected by Swift in the direction of the constellation Draco with the peak luminosity 10^{48} erg s $^{-1}$ (see Fig. 2). Observations showed that the transient originated from the center of a galaxy at cosmological distances involving a SMBH in the galaxy nucleus. It was concluded that Swift J164449.3+573451 is most likely originated from the central SMBH, and the X-ray and radio emissions were interpreted as a result of stellar capture by the black hole (see, e.g., Levan et al. 2011; Burrows et al. 2011; Zauderer et al. 2011).

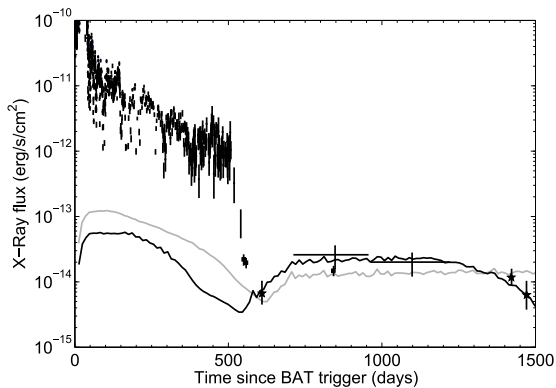


Figure 2. The observed X-ray light curve of Swift J1644+57 from Swift, XMM-Newton and Chandra. Figure reproduced from Cheng et al. (2016) with permission.

2. STRUCTURE OF THE FERMI BUBBLES

A sudden (sporadic) energy release by a TDE in the GC creates a cavity with a shock which expands into the surrounding non-uniform medium of the halo. For example, the gas distribution in the halo above (and below) the Galactic plane is decaying exponentially with a scale height $H = 2$ kpc and the density at the plane is $n_0 = 4 \times 10^{-3}$ cm $^{-3}$ (see, e.g., Nakashima et al. 2019). The exponential gas distribution is

$$\mathcal{R}(z) = \exp\left(-\frac{z}{H}\right), \quad (1)$$

where $\mathcal{R}(z) = n(z)/n_0$.

Alternatively, Miller & Bregman (2016) suggested a so-called β -model of the gas density profile in the halo

from the intensity of absorption lines,

$$\mathcal{R}(z) = \left(\frac{z}{z_c}\right)^{-3\beta}, \quad (2)$$

where $z_c = 0.26$ kpc and $n_0 = 0.5$ cm $^{-3}$.

The formalism of envelope propagation was developed as a solution for a strong explosion (see Sedov 1959), and was elaborated by Kompaneets (1960) for explosion in a non-uniform atmosphere. The reader is referred to the review of Bisnovaty-Kogan & Silich (1995) and the monograph of Zel'dovich & Raizer (1967). This model was derived for the thermonuclear explosion in the terrestrial atmosphere. Fig. 3 shows an example of a thermonuclear explosion test in the terrestrial atmosphere.



Figure 3. A thermonuclear explosion in the terrestrial atmosphere. Image credit: United States Department of Energy. Image from [https://commons.wikimedia.org/wiki/File:Castle_Bravo_nuclear_test_\(cropped\).jpg](https://commons.wikimedia.org/wiki/File:Castle_Bravo_nuclear_test_(cropped).jpg).

Kahn (1998), Baumgartner & Breitschwerdt (2013), Ko et al. (2020) and Schulreich & Breitschwerdt (2022) developed analytical solutions of a hydrodynamic model for the shock wave propagation in non-uniform atmospheres or halos, for different energy input rates for single and successive explosions. The shock envelope generated has a double-bubble structure in the halo (see Fig. 4).

Following the Kompaneets formalism (see details in Bisnovaty-Kogan & Silich 1995), the shock front is described as

$$\left(\frac{\partial r}{\partial y}\right)^2 - \frac{1}{\mathcal{R}(z)} \left[\left(\frac{\partial r}{\partial z}\right)^2 + 1 \right] = 0, \quad (3)$$

where $y(t)$ is a transformed time (in units of length)

$$y = \int_0^t \sqrt{\frac{(\gamma_g^2 - 1)}{2} \frac{2\mathcal{E}(t)}{3\rho_0 V(t)}} dt, \quad (4)$$

$V(t)$ is the bubble volume

$$V(t) = \pi \int_0^{z_u} r^2(z, t) dz, \quad (5)$$

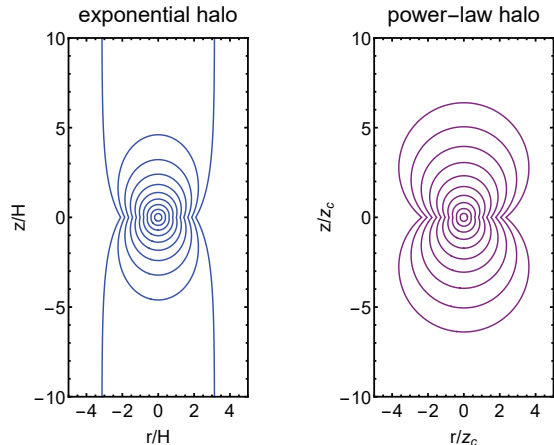


Figure 4. Illustration of the double-bubble shock envelope in the halo evolving with time. The gas distribution in the halo in the left panel is exponential and in the right panel is power-law. Figure adapted from [Ko et al. \(2020\)](#) with permission.

with $r(z, t)$ or $r(z, y)$ as the bubble radius at the altitude z , $\rho_0 = n_0 m_p$ is the mass density corresponding to n_0 (the number density at the base $z = 0$), \mathcal{E} is the energy released by the central source into the bubble, and γ_g is the adiabatic index of the gas.

For the exponential gas distribution given by Eq. (1), the top of the bubble z_u is a function of time t ,

$$z_u = -2H \ln \left(1 - \frac{y}{2H} \right). \quad (6)$$

In this model of [Baumgartner & Breitschwerdt \(2013\)](#) and [Schulreich & Breitschwerdt \(2022\)](#) the velocity at the top of the bubble v_u for the total energy release of \mathcal{E} is

$$v_u = \frac{dz_u}{dt} = \exp \left(\frac{z_u}{2H} \right) \frac{dy}{dt}. \quad (7)$$

In the early phase when $z_u \lesssim H$, the expanding cavity can be described by the Sedov solution ([Sedov 1959](#)) when the gas density is almost uniform and the velocity of the shock envelope decreases with time. When $z_u > H$ the shock propagates in the exponential halo with acceleration afterwards (see [Baumgartner & Breitschwerdt 2013](#)).

The propagation of the shock envelope is derived under the strong shock assumption. In reality, if the velocity of the envelope is below the sound speed c_s of the halo gas, then the shock or the envelope will decay and be absorbed in the halo. On the other hand, if this velocity is higher than the sound speed, the shock will be able to penetrate into the halo, and transfer the energy from the initial central source into the exponential halo. The velocity of the top of the bubble is the fastest, [Baumgartner & Breitschwerdt \(2013\)](#) defined a condition of shock penetration into the exponential halo: $v_u(y_{\text{acc}}) > 3c_s$, where $v_u(y_{\text{acc}})$ is the minimum of v_u

and this occurs at $y = y_{\text{acc}}$, i.e., $\dot{v}_u(y_{\text{acc}}) = \ddot{z}_u(y_{\text{acc}}) = 0$. The acceleration at the top of the bubble is (see [Baumgartner & Breitschwerdt 2013](#)),

$$\ddot{z}_u = \frac{H}{t_{\text{SN}}^2} \frac{(\gamma_g^2 - 1)}{4(1 - \tilde{y}/2)\tilde{V}} \left[\frac{1}{(1 - \tilde{y}/2)} - \frac{1}{\tilde{V}} \frac{d\tilde{V}}{d\tilde{y}} \right], \quad (8)$$

where

$$\tilde{y} = \frac{y}{H}, \quad \tilde{V} = \frac{V}{H^3}, \quad t_{\text{SN}} = \sqrt{\frac{3\rho_0 H^5}{2\mathcal{E}_{\text{SN}}}}. \quad (9)$$

As an example we present in the left panel of Fig. 5, the development of the shock velocity at the top of the bubble from a single energy explosion \mathcal{E} . The energy of the explosion occupies more and more volume of the exponential atmosphere, and finally approaching infinity in finite time (provided that the velocity is always larger than $3c_s$).

For the parameters in the GC, a single star disruption event provides no more than $10^{52} \sim 10^{53}$ erg (see [Piran et al. 2015; Dai et al. 2018, 2021](#)). There is not enough energy for the FBs or similar structures. An unusually huge single energy release in the past, say exceeding $\mathcal{E} > 10^{54}$ erg, may explain the origin of the Fermi Bubbles.

Alternatively, this huge energy can be supplied by a series of many weaker disruption events with an effective power input $\dot{\mathcal{E}} \geq 10^{40}$ erg s^{-1} , see the right panel of Fig. 5. It may be interpreted as routine TDEs of which each produced an energy of $10^{52} \sim 10^{53}$ erg, and the average rate of stellar capture is about $10^{-5} \sim 10^{-4}$ yr^{-1} (see [Ko et al. 2020](#)).

The envelope shell is composed of the swept-up gas of the bubble, and it is much thinner in comparison to the size of the bubble. The shell thickness is defined as

$$d(y) = \frac{M_s(y)}{2\pi\rho_{\text{sh}0} \int_0^{z_u(y)} e^{-z/H} r(z, y) \sqrt{1 + \left(\frac{\partial r}{\partial z} \right)^2} dz}, \quad (10)$$

where M_s is the total mass of the FB

$$M_s(y) = \pi\rho_0 \int_0^{z_u(y)} e^{-z/H} r^2(z, y) dz, \quad (11)$$

and $\rho_{\text{sh}} = \rho_{\text{sh}0} \exp(-z/H)$ is the density within the shell (see [Schulreich & Breitschwerdt 2022](#)).

Fig. 6 shows some examples of numerical simulation of the FB envelope from sporadic star disruption or from a single huge explosion.

3. ENVELOPE DISRUPTION BY RAYLEIGH-TAYLOR INSTABILITY

The interface between a denser fluid supported by a lighter fluid in a gravitational field is susceptible to Rayleigh-Taylor (RT) instability. The amplitude of an

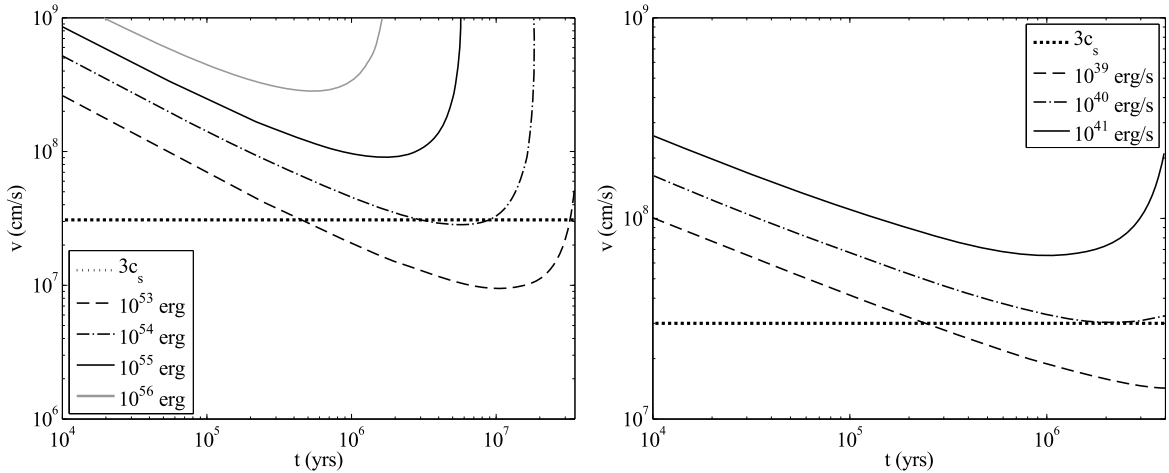


Figure 5. Temporal variation of the shock velocity of the top of the bubble for the case of exponential halo with $H = 0.67$ kpc and $n_0 = 0.03 \text{ cm}^{-3}$. *Left panel:* One single input of energy from the GC. *Right panel:* Multiple TDEs with different values of the power release at the GC. The horizontal dotted line indicates the velocity which is necessary for the shock in order not to stall in the halo. It is three times the sound speed in the halo $3 \times 10^7 \text{ cm s}^{-1}$. Figure reproduced from Ko et al. (2020) with permission.

infinitesimal perturbation will grow exponentially at the early phase or the linear phase (see, e.g., Chandrasekhar 1961). The growth time of the instability in linear phase is

$$\tau_{\text{RT}} = \sqrt{\frac{\lambda}{2\pi g} \frac{(\rho_2 + \rho_1)}{(\rho_2 - \rho_1)}}, \quad (12)$$

where λ is the wavelength of the perturbation, g is the gravitational acceleration and ρ_1 and ρ_2 are the densities of the lighter and denser fluids, respectively. For an illustration of time evolution of the RT instability, the reader is referred to Figure 4 of Schulreich & Breitschwerdt (2022).

In the case of a superbubble, the RT instabilities are excited between the dense shell and the hot interior when the envelope is accelerating into the exponential halo (see Baumgartner & Breitschwerdt 2013; Schulreich & Breitschwerdt 2022, and Eq. (8)). Identifying the gravitational acceleration with the acceleration at the top of the bubble $\ddot{z}_u(y)$ gives the growth time of the instability (in this coordinates)

$$\tau_{\text{RT},z_u}(y) = \sqrt{\frac{d(y)}{2\pi\ddot{z}_u(y)} \frac{[\rho_{\text{sh}}(y) + \rho_{\text{in}}(y)]}{[\rho_{\text{sh}}(y) - \rho_{\text{in}}(y)]}}, \quad (13)$$

where y is the transformed time (see Section 2). When the wavelength λ of the RT fluctuations is about the envelope shell thickness d , these instabilities may destroy the bubble, see Figure 13 of Schulreich & Breitschwerdt (2022).

The temporal evolution of the RT instability during the nonlinear regime is obtained by numerically solving the ordinary differential equation for the RT fluctuations of λ ,

$$\dot{\lambda}(y) = 2\sqrt{\alpha\ddot{z}_u(y)\lambda(y)}. \quad (14)$$

The parameter α is estimated from the initial condition $\lambda(y_0) \sim 0.01d(y_0)$ (see Baumgartner & Breitschwerdt 2013).

4. ENERGY AND SPECTRUM OF HYDRODYNAMIC FLUCTUATIONS

From Eq. (14) we can estimate the fraction of the total energy of the FBs, $\dot{\mathcal{E}} \sim 3 \times 10^{41} \text{ erg s}^{-1}$, that is transformed into the hydrodynamic turbulence in the envelope excited by the RT instabilities there. From Landau & Lifshitz (1987) we get the rate of energy dissipation in the turbulent of flux

$$\varepsilon(t) = \frac{v_\lambda^3}{\lambda}. \quad (15)$$

Instead of λ we can introduce a wavenumber $k = 2\pi/\lambda$. (the Kolmogorov-Obukhov spectrum of turbulence). Then the kinetic energy spectrum $W(k)$ of the turbulence is

$$W(k) \sim \varepsilon^{2/3} k^{-5/3}, \quad (16)$$

and

$$\int_k^\infty W(k) dk \sim v_\lambda^2. \quad (17)$$

In this case a universal energy spectrum $W(k)$ is developed in the inertial range as shown in Eq. (16), i.e., the Kolmogorov-Obukhov spectrum of turbulence Landau & Lifshitz (1987).

The energy losses of RT, $\varepsilon(t)$, in the envelope, transferred into the turbulence, is

$$\varepsilon(t) = \frac{\dot{\lambda}_0^3(t)}{\lambda_0(t)} = 8\alpha^{3/2}\ddot{z}_u^{3/2}\lambda_0^{1/2}, \quad (18)$$

where $\lambda_0 = 2\pi/k_0$ is the pumping scale (see below).

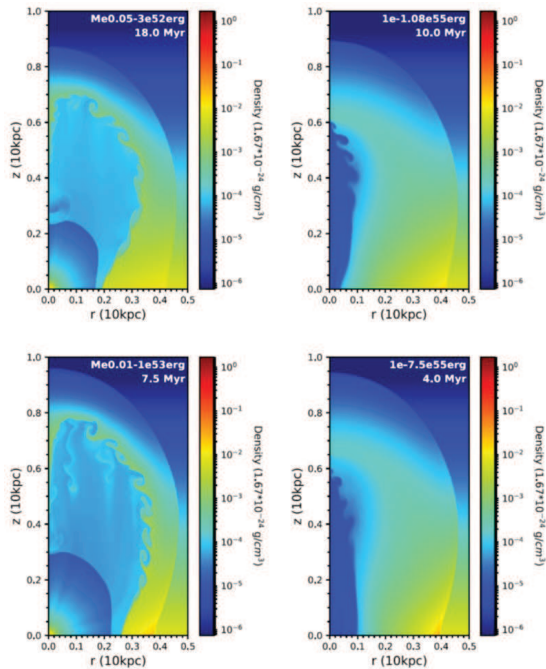


Figure 6. Density distribution of numerical simulations of the FBs in an exponential halo. The two panels on the left column are results of multiple explosions (e.g., TDEs) and the right column are results of a single huge explosion. In the upper left panel, “Me0.05-3e52erg 18.0 Myr” corresponds to multiple explosions with 0.05 Myr between successive explosions and the energy release by each explosion is 3×10^{52} erg, and the simulation ends at 18.0 Myr. In the upper right panel, “1e-1.08e55erg 10.0 Myr” corresponds to a single explosion with an energy release of 1.08×10^{55} erg, and the simulation ends at 10.0 Myr. Similar explanation for the lower panels. Lower panel figures reproduced from Ko et al. (2020) with permission.

The spectrum of hydrodynamic fluctuations $W(k)$ has a wide inertial interval, where the energy is supplied in the initial scale of $k_0 < k$, in which only energy transfer along the spectrum is realized. In the energy range the spectrum at $\lambda < \lambda_0 = 2\pi/k_0$ is determined only by the power of energy pumping at the scale λ_0 .

The growth of this large-scale structure may be understood at each stage in terms of ring vortex pairing, mutual orbiting, and merging, followed by these processes repeating with the just merged eddies on a larger scale. During this development, ambient material is entrained and intense smaller scale turbulence is generated in the regions between the vortices, presumably establishing the turbulent cascade to higher wavenumbers, which is eventually dominated by viscosity on the Kolmogorov microscale, l_K . The small-scale of the stretched turbulence-generating regions between the vortices can be associated with the Taylor microscale, l_T .

The total fluid turbulence energy is given by $E_t = \rho v_t^2$, where ρ is the fluid density and v_t is the root mean square of the velocity of the turbulence (or simply the turbulence velocity) at the largest scale λ_0 or l_0 . The range is taken to extend from l_0 , down to the effective damping (or Kolmogorov) scale l_K . The Reynolds number in this case is,

$$Re = \left(\frac{l_0}{l_K} \right)^{4/3}, \quad (19)$$

where the smallest scale, l_K , is defined by the dissipation of turbulence.

There is no absolute definition of the scale l_T of this transition from hydrodynamic spectrum to that of MHD (upper limit of MHD-turbulence scale). Following Eilek & Hendriksen (1984) the Taylor length, l_T , was estimated as

$$l_T \sim l_0 \left(\frac{15}{Re} \right)^{1/2}. \quad (20)$$

Therefore, the fluid cascade extends from the Taylor scale l_T , on which the transition from a large-scale ordered turbulence to smaller scale disordered motion occurs. The cascade proceeds down to the smallest scale l_K , determined by dissipation,

$$l_K \approx l_0 (Re)^{-3/4}. \quad (21)$$

We adopt the hydrodynamic view that the Kolmogorov equilibrium cascade exists between l_T and l_K as our first approximation to the complex interactions expected in the regime. The relation between (the root mean square of) the turbulence velocity $v(l)$ and the turbulence scale l is

$$v(l) = v(l_T) \left(\frac{l}{l_T} \right)^{1/3}. \quad (22)$$

5. PARTICLE ACCELERATION BY ALFVÉN FLUCTUATIONS AND THE LIGHTHILL RADIATION

Contrary to shock acceleration, the turbulent resonant acceleration does not require strong shocks. The fluid turbulence in the interstellar medium or intercluster medium is another possible origin of particle acceleration, e.g., in galaxy clusters (Brunetti et al. 2004), and in radio jets in turbulent mixing regions (Hendriksen et al. 1982). Turbulent motions act as a source of waves which is presented as a hierarchy of eddies. The Lighthill mechanism acts as a direct source of energy to the MHD waves over the range of wavenumbers corresponding to the fluid turbulent spectrum. A turbulent eddy has kinetic energy, which it releases when it mixes with its surroundings. Most of this energy is returned to the ambient medium, but a small fraction gets transformed into propagating waves (see, e.g., Stein

1981; Hendriksen et al. 1982; Blasi 2000; Brunetti et al. 2001; Fujita et al. 2003, and others). A strong coupling between particle energy and turbulent energy spectra can be expected, and the hydrodynamic turbulence in the medium accelerates particles through wave-particle resonance. Alfvén waves is an alternative source of charged particle acceleration via resonant interaction of MHD-waves and with relativistic particles.

In the pioneering paper Lighthill (1952) developed the model of acoustic waves which are excited by hydrodynamic turbulence in the absence of magnetic fields. This is known as the Lighthill radiation. The radiated power of the waves is roughly the energy density in the turbulent motion, ε , divided by the decay time scale of waves τ , and the compactness of the eddy (which is measured by the ratio of the size of the eddy, l , to the wavelength, $\lambda = 2\pi/k$).

Kulsrud (1955) showed that this radiation of MHD-turbulence is excited if there is an external constant magnetic field. If there is no external magnetic field, the magnetic turbulence generates sound waves only via the Lighthill mechanism. If there is a constant external magnetic field, hydromagnetic waves are generated instead by Alfvén waves unless the energy density of hydrodynamic turbulence prevails over the energy of magnetic density. The central idea was a coupling between the hydrodynamic eddy cascade and the MHD waves through the process of Lighthill radiation is presented in Kulsrud (1955), Parker (1964) and Kato (1968).

Kato (1968) developed the Lighthill theory of the MHD-radiation for strong and weak magnetic fields B which is characterized by the magnetic Mach number, the ratio of the (root mean square) velocity of the hydrodynamic turbulence v to the Alfvén speed $v_A = B/\sqrt{4\pi\rho}$,

$$M_A = \frac{v}{v_A}. \quad (23)$$

For small Mach numbers ($M_A \ll 1$) a small fraction of the power emitted is in the form of Alfvén waves, while for large Mach numbers ($M_A \gg 1$) the power emits as sound waves and the radiation of Alfvén waves is insignificant. The turbulence decay time scale is the nonlinear cascade time, which is the eddy turnover time, i.e., the eddy size l divided by its velocity v ,

$$\tau \approx \frac{l}{v}. \quad (24)$$

For Alfvén waves in strong magnetic field, and the frequency is $\omega = \bar{k}v_A$, and

$$\bar{k}l \approx \frac{v}{v_A}, \quad (25)$$

which corresponds to the resonance $\tau(l) \approx 1/\omega(\bar{k})$.

From radio polarization measurements, Zhang et al. (2024) showed that there are large-scale magnetic fields in the Fermi and eROSITA bubbles. Figure 1 of

Zhang et al. (2024) showed several kpc-scale magnetised structures in the bubbles.

If the turbulent magnetic field dominates the motion ($M_A \ll 1$), then the power is

$$P_A \sim \frac{\rho v^3}{l} M_A, \quad (26)$$

and a small fraction of flux of hydrodynamic is transformed into Alfvén waves. In the following we present some details of the radiation of MHD-waves in space medium in the limit of strong external magnetic fields.

We assume that fluid turbulence is induced by the motion of a smaller cluster in a larger cluster and its energy spectrum is described by a power law (see Eilek & Hendriksen 1984; Fujita et al. 2003)

$$W_f(k) = W_f^0 k^{-m}, \quad (27)$$

where $k = 2\pi/l$ is the wavenumber corresponding to the scale l , $W_f(k)\delta k$ is the energy per unit volume in turbulence with wavenumbers between k and $k + \delta k$, and W_f^0 and m are the constants. If one expresses the turbulent spectrum in terms of eddy size, the spectrum is represented by $W(l) \propto l^{m-2}$. The cascade of the fluid turbulence extends from a largest eddy size $l_0 = 2\pi/k_0$ down to a smallest scale determined by dissipation $l_K \sim l_0 Re^{-3/4}$ (where Re is the Reynolds number). Since most of the energy of fluid turbulence resides in the largest scale, the total energy density of fluid turbulence is presented in the form as $E_t \sim \rho v_t^2$, where ρ is the fluid density and v_t is the turbulent velocity of the largest scale l_0 . The normalization W_f^0 can be derived from the relation $E_t = \int_{k_0}^{k_T} W_f(k) dk$,

$$W_f^0 = \frac{E_t}{R} k_T^{(m-1)}, \quad (28)$$

where

$$R = \frac{1}{(m-1)} \left[\frac{k_0 W_f(k_0)}{k_T W_f(k_T)} - 1 \right] \\ \approx \frac{1}{(m-1)} \frac{k_0 W_f(k_0)}{k_T W_f(k_T)}. \quad (29)$$

Here $k_T = 2\pi/l_T$ and l_T is the wavelength below which Alfvén waves are driven.

A fluid eddy of size l has a velocity

$$v(l) \approx \left[\frac{l W_f(l)}{\rho} \right]^{1/2} = \left[\frac{k W_f(k)}{\rho} \right]^{1/2} \\ = \left(\frac{E_t}{\rho R} \right)^{1/2} \left(\frac{k}{k_T} \right)^{(1-m)/2}. \quad (30)$$

Turbulence on a scale k will radiate Alfvén waves at the wavenumber

$$\bar{k} = \left[\frac{v(l)}{v_A} \right] k, \quad (31)$$

Here we recall that k is the wavenumber of hydrodynamic turbulence and \bar{k} is the wavenumber of the Alfvén waves.

Let $v[k(\bar{k})]$ be the fluid velocity on the fluid scale $k(\bar{k})$ that drives Alfvén waves of wavenumber \bar{k} . From equations (30) and (31), we obtain

$$v[k(\bar{k})] = v_A \left[\frac{E_t}{\rho v_A^2 R} \left(\frac{\bar{k}}{k_T} \right)^{(1-m)} \right]^{1/(3-m)}. \quad (32)$$

Assuming that the energy going into Alfvén waves at wavenumber \bar{k} with an energy flux

$$I_A(\bar{k}) = I_0(\bar{k}/k_T)^{-s_t}, \quad (33)$$

where $I_A(\bar{k})\delta\bar{k}$ is the power per unit volume going into Alfvén waves with wavenumbers in the range $\bar{k} \rightarrow \bar{k} + \delta\bar{k}$ and I_0 and s_t are the constants. In this case, the power per unit volume going into the Alfvén mode from fluid turbulence is

$$P_A = \int_{\bar{k}}^{\bar{k}_{\max}} I_A(\bar{k}) d\bar{k} \approx \frac{I_0 k_T}{(s_t - 1)} \left(\frac{\bar{k}}{k_T} \right)^{(1-s_t)}, \quad (34)$$

where $\bar{k} \ll \bar{k}_{\max}$ and $s_t > 1$.

On the other hand, according to the Lighthill theory, P_A is given by (cf. Eq. (26))

$$P_A = \eta_A \left[\frac{v(l)}{v_A} \right] \rho v^3(l) k, \quad (35)$$

where η_A is an efficiency factor of order unity (Kato 1968; Hendriksen et al. 1982; Eilek & Hendriksen 1984). By comparing Eqs. (34) & (35), and using Eqs. (31) & (32), we obtain (see Eilek & Hendriksen 1984; Fujita et al. 2003),

$$s_t = \frac{3(m-1)}{(3-m)}, \quad (36)$$

$$I_0 = \eta_A (s_t - 1) \rho v_A^3 \left(\frac{E_t}{\rho v_A^2 R} \right)^{3/(3-m)}. \quad (37)$$

The power radiated in the form of Alfvén waves P_A is dominated by small \bar{k} and the smallest is \bar{k}_T . With Eq. (30) and $\bar{k}_T = [v(l_T)/v_A] k_T$, the total power in the form of Alfvén waves is approximately,

$$P_A = \eta_A \left(\frac{E_t}{\rho v_A^2 R} \right)^2 \rho v_A^3 k_T. \quad (38)$$

For Kolmogorov turbulence, the spectral index is $m = 5/3$ (see Eq. 27), and the spectral index of Alfvén wave flux is $s_t = 3/2$ (Eq. 33).

6. SPECTRUM OF MHD TURBULENCE IN THE FERMI BUBBLE ENVELOPE

The evolution of the spectrum of the Alfvén waves, $W_k(t)$ is described by the equation of nonlinear diffusion presented in, e.g., Brunetti et al. (2004) and Brunetti & Blasi (2005),

$$\frac{\partial W_k(\bar{k}, t)}{\partial t} = \frac{\partial}{\partial \bar{k}} \left[D_{kk} \frac{\partial W_k(\bar{k}, t)}{\partial \bar{k}} \right] - \Gamma(\bar{k}) W_k(\bar{k}, t) + I_A(\bar{k}, t). \quad (39)$$

The first term on the right hand side of Eq. (39) describes the nonlinear MHD wave-wave cascade. The diffusion coefficient for the Kolmogorov and the Iroshnikov-Kraichnan spectra (e.g., Miller & Roberts 1995)

$$D_{kk} = v_A \begin{cases} \bar{k}^{7/2} \left[\frac{W_k(\bar{k}, t)}{2W_B} \right]^{1/2}, & \text{Kolmogorov} \\ \bar{k}^4 \left[\frac{W_k(\bar{k}, t)}{2W_B} \right], & \text{Iroshnikov-Kraichnan} \end{cases} \quad (40)$$

where $W_B = B_0^2/8\pi$.

The second term on the right hand side of Eq. (39) describes the damping of MHD-waves by collisions of relativistic and thermal particles in the interstellar or intercluster medium (see Eilek 1979)

$$\begin{aligned} \Gamma_k &\simeq \frac{4\pi^3 e^2 v_A^2}{\bar{k} c^2} \int_{p_{\min}}^{p_{\max}} p^2 (1 - \mu_\alpha) \frac{\partial F(p, t)}{\partial p} dp \\ &= \frac{\pi^2 e^2 v_A^2}{\bar{k} c^2} \int_{p_{\min}}^{p_{\max}} (1 - \mu_\alpha) \\ &\quad \times \left[\frac{\partial N(p, t)}{\partial p} - \frac{2N(p, t)}{p} \right] dp, \end{aligned} \quad (41)$$

where $F(p, t)$ is the particle distribution function and $N(p, t) = 4\pi p^2 F(p, t)$, and

$$\mu_\alpha = \frac{v_A}{c} \pm \frac{m\Omega}{p\bar{k}}. \quad (42)$$

Here the upper and lower signs are for negative and positive charged particles, respectively.

The third term on the right hand side of Eq. (39), I_A , describes the injection of Alfvén waves by the fluid turbulence through the Lighthill mechanism.

The time scale of the damping with the thermal pool is considerably shorter than the cascade time scale for $\bar{k}/\bar{k}_{\max} \gg 0.1$. Thus, a break or a cutoff in the wave spectrum is expected at large wavenumbers.

In the following, we present an alternative formulation of the steady-state equation for $W_k(\bar{k})$. For simplicity it is described in a compact form (see Norman & Ferrara 1996; Ptuskin et al. 2006, and references therein)

$$\frac{\partial}{\partial \bar{k}} \left(\frac{\bar{k} W_k}{T_{\text{NL}}} \right) = 2\Gamma_{\text{CR}} W_k + I_A(\bar{k}). \quad (43)$$

Here the source of MHD-fluctuations, $I_A(\bar{k})$, is given by Eq. (33).

The rate of damping MHD-waves by cosmic rays, $\Gamma_{\text{CR}}(\bar{k})$, is (see, e.g., Berezinsky et al. 1990)

$$\Gamma_{\text{CR}}(\bar{k}) = \frac{\pi Z^2 e^2 v_A^2}{2\bar{k}c^2} \int_{p_{\text{res}}(\bar{k})}^{\infty} \frac{dp}{p} F(p), \quad (44)$$

where $F(p)$ is the CR distribution, p is the particle momentum, and $p_{\text{res}}(\bar{k}) = ZeB/c\bar{k}$.

In the form of the Iroshnikov-Kraichnan spectrum, the term of the left hand side of Eq. (43) is

$$\frac{\partial}{\partial \bar{k}} \left(\frac{\bar{k}W_k}{T_{\text{NL}}} \right) = \frac{d}{d\bar{k}} \left[\frac{C(\bar{k}^3 W^2(\bar{k}))}{\rho v_A} \right], \quad (45)$$

where the interaction is

$$T_{\text{NL}}^{-1}(\bar{k}) = C_{\text{NL}} \frac{\bar{k}^2 W_k(\bar{k})}{m_i n_i v_A}, \quad (46)$$

and the constant $C_{\text{NL}} \sim 1$.

If the magnetic field fluctuations are injected by an external source at the scale $L = 1/\bar{k}_L$, Eq. (43) can be simplified to

$$\frac{\partial}{\partial \bar{k}} \left(\frac{\bar{k}W_k}{T_{\text{NL}}} \right) = 2\Gamma_{\text{CR}}W_k + \Phi \delta(\bar{k} - \bar{k}_L). \quad (47)$$

This result has been applied to the spectrum of MHD-turbulence in the FB envelope for $\bar{k} > \bar{k}_0$ (Cheng et al. 2014). The solution of Eq. (47) is given by

$$W_k(\bar{k}) = \left(\frac{\bar{k}_0}{\bar{k}} \right)^{3/2} W_k(\bar{k}_0) - \frac{Z^2 e^2 B^2 v_A}{8C c^2 \bar{k}^{3/2}} \int_{\bar{k}_0}^{\bar{k}} \bar{k}_L^{-5/2} d\bar{k} \int_{p_{\text{res}}(\bar{k}_L)}^{\infty} \frac{F(p)dp}{p}, \quad (48)$$

where $W_k(\bar{k}_L) = \bar{k}_L^{-3/2} \sqrt{\rho v_A \Phi / C}$, where Φ describes the source injection at \bar{k}_L .

The coefficient of momentum diffusion of CRs is (see Berezinsky et al. 1990)

$$D_p(p) = p^2 \kappa(p), \quad (49)$$

where

$$\kappa(p) = \frac{3\bar{k}_{\text{res}}^2 W_k(\bar{k}_{\text{res}})}{\rho v}. \quad (50)$$

Here $\bar{k}_{\text{res}} = 1/r_L = ZeB/pc$, r_L is the particle Larmor radius, B is the magnetic field strength.

The momentum diffusion coefficient D_p for the Bubble parameters is shown in Fig. 7 (solid line). For comparison the dash-dotted line is the diffusion coefficient for the Kraichnan spectrum of turbulence without CR absorption.

As shown in Fig. 7, the wave damping by cosmic rays can terminate the cascade for relatively small CR

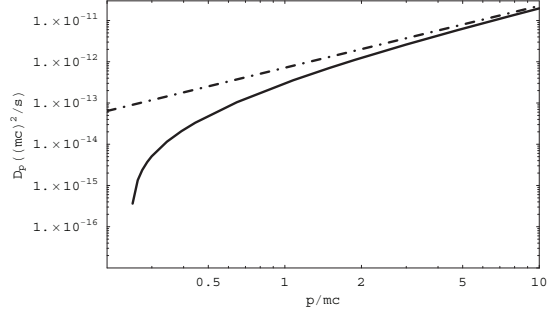


Figure 7. The solid line shows the momentum diffusion coefficient derived for the bubble parameters when the CR absorption is taken into account. The dash-dotted line is the results ignoring the CR absorption. Figure reproduced from Cheng et al. (2014) with permission.

momenta p . Brunetti et al. (2004) showed that the time of damping was considerably shorter than the cascade time for large wavenumbers. They concluded also that the damping rate on protons largely dominates that on electrons. These protons can exhibit a resonance with the relativistic electrons which may be important for their acceleration.

From Eqs. (48), the distribution function of CR electrons, $F(p)$, can be estimated from the observed gamma-ray (Su et al. 2010; Ackermann et al. 2014) and microwave (Planck Collaboration 2013) emissions for the expected parameter of FB envelope of hydrodynamic turbulence.

If the effect of CR damping is insignificant and $2\Gamma_{\text{CR}}W_k$ can be ignored in Eq. (43), then Eq. (43) is simply the balance of wave cascading and MHD-excitation by the hydrodynamic turbulence,

$$\frac{\partial}{\partial \bar{k}} \left(\frac{\bar{k}W_k}{T_{\text{NL}}} \right) \approx I_A(\bar{k}). \quad (51)$$

With Eq. (33), the spectrum of MHD-fluctuations W_k is

$$W_k^2(\bar{k}) \approx \frac{\rho v_A}{C_{\text{NL}} \bar{k}^3} \left[\mathcal{P}_0 - \frac{I_0 k_0}{(s_t - 1)} \left(\frac{k_0}{\bar{k}} \right)^{(s_t - 1)} \right], \quad (52)$$

where

$$\mathcal{P}_0 = \frac{I_0 k_0}{(s_t - 1)} + \frac{C_{\text{NL}}}{\rho v_A} k_0^3 W_k^2(k_0). \quad (53)$$

A cutoff in the spectrum of the waves W_k can be estimated from the balance between damping and the cascade at large wavenumbers.

In contrast to the classical GALPROP code with accepted arbitrarily parameters of the kinetic diffusion (see, e.g., Moskalenko & Strong 1998; Porter et al. 2008; Vladimirov et al. 2011), we derive the coefficients of the kinetic equation for CRs in the FB envelope from Eq.

(47) for the MHD-turbulence,

$$\begin{aligned} & \frac{\partial F(p)}{\partial t} + \frac{F(p)}{\tau_{\text{esc}}} - Q(p, z) \\ &= \frac{1}{p^2} \frac{\partial}{\partial p} p^2 \left[D_p(p) \frac{\partial F(p)}{\partial p} - \left(\frac{dp}{dt} \right) F(p) \right] \\ & \quad + \frac{\partial}{\partial z} D_{zz}(p) \frac{\partial F(p)}{\partial z}, \end{aligned} \quad (54)$$

where (dp/dt) (> 0) is the rate of continuous energy losses, τ_{esc} is catastrophic CR losses or the characteristic time of CR escape from the envelope, $Q(p, z)$ is the internal sources of CRs, D_{zz} is the coefficient of spatial diffusion

$$D_{zz}(p) = \frac{vB^2}{6\pi^2 k^2 W_k(\bar{k})} = \frac{2\rho v_A^2 v}{3\pi k^2 W(\bar{k})}, \quad (55)$$

and D_p is the coefficient of momentum diffusion and is described by Eqs. (49) and (50). Here $\bar{k} = 1/r_L = ZeB/pc$ (cf. Eqs. (49) & (50)).

Our goal is to derive the spectrum of CRs from a combination of kinetic MHD/CR equations and to estimate the proper and correct coefficients of Eq. (54). However, there is still a gap between the correct coefficients of the kinetic equations and some rough estimations of the spatial and momentum diffusions from the observed gamma-ray and microwave emissions from the FBs. At present we are unable to derive reliable numerical values of these coefficients, and try to estimate roughly these parameters from the data ignoring the equation for the origin of MHD turbulence needed for CR scattering and propagation. These parameters of the spatial and momentum diffusion coefficients were roughly or arbitrarily estimated, e.g., by weak random waves of a hydromagnetic turbulence (see [Mertsch & Sarkar 2011](#)), by a supersonic turbulence (see [Bykov & Toptygin 1993](#)), or by simple estimations of electron acceleration from shocks of the FBs (see [Cheng et al. 2011](#)), etc.

In the following, we describe how to roughly estimate the parameters of the spatial and momentum diffusion coefficients from the observed gamma-ray and microwave emissions from the FBs.

7. LEPTONIC AND HADRONIC ORIGINS OF THE RADIATION FROM THE FERMI BUBBLES

The origin of CRs in the envelope of the giant bubbles is still an open question. The structure of the bubbles is complicated. It is seen in thermal X-ray as an outer envelope with the parameters:

- Power of hydrodynamic turbulence $\sim 10^{39}$ erg s⁻¹
- Thickness of the envelope ~ 100 pc
- Scale of eROSITA bubbles ~ 14 kpc
- Magnetic field $\sim 8 \times 10^{-6}$ G
- Gas density $\sim 4 \times 10^{-3}$ cm⁻³
- Alfvén velocity $\sim 3 \times 10^7$ cm s⁻¹

An inner envelope of size about ~ 8 kpc is seen in the nonthermal gamma-ray and microwave emissions (see Fig. 8). The microwave emission is evidently produced by the synchrotron losses of relativistic electrons, while the origin of gamma-rays is not clear.

The total gamma-ray luminosity of the bubbles between 100 MeV and 500 GeV is $F_\gamma \simeq 4.4 \times 10^{37}$ erg s⁻¹ (see [Ackermann et al. 2014](#)). The spectrum can be described by a power-law $dF_\gamma/dE_\gamma \propto E_\gamma^{-1.87}$ with a cut-off $E_{\text{cut}} \simeq 113$ GeV.

7.1. Origin of gamma-ray emission from the Fermi Bubbles

The spectrum of gamma-rays can be fitted by either leptonic or hadronic model.

- Leptonic model: The rate of gamma-rays production by relativistic electrons interacting with the low-energy interstellar photons is given by (see [Ackermann et al. 2014](#))

$$\begin{aligned} \varepsilon_{\text{IC}}(E_\gamma) &= c \sum_i n_i(\epsilon_{\text{ph}}) \\ & \times \int \frac{d\sigma_{\text{IC}}(E_\gamma, E_e, \epsilon_{\text{ph}})}{dE_\gamma} N_e(E_e) dE_e, \end{aligned} \quad (56)$$

where σ_{IC} is the inverse Compton (IC) cross-section (see, e.g., [Moskalenko et al. 2006](#)). The parameters of the CR electron spectrum was derived from the observed gamma-ray emission from the envelope: $N_e \propto E_e^{-2.17}$, $E_{\text{cut}} \sim 1.25$ TeV. The required total energy in electrons above 1 GeV is $\mathcal{E}_e \sim 10^{52}$ erg.

- Hadronic model: gamma-ray can be produced by proton-proton (p-p) collisions. For the calculations of the emission from p-p collision, [Ackermann et al. \(2014\)](#) used the p-p cross-section from [Kamae et al. \(2006\)](#). The rate of gamma-ray production by p-p collisions is

$$\varepsilon_{\text{pp}}(E_\gamma) = c \int \frac{d\sigma_{\text{pp}}(E_\gamma, E_p)}{dE_\gamma} n_H N_p(E_p) dE_p. \quad (57)$$

The required spectrum of CR protons is expressed as $dN_p/dE_p \propto E_p^{-2.13} \exp(-E_p/E_{\text{cut}})$, where $E_{\text{cut}} \sim 14$ TeV. The needed total energy in CR protons above 1 GeV is $\mathcal{E}_p \sim 3.5 \times 10^{55}$ erg for $n_H = 0.01$ cm⁻³.

In principle, we can interpret the gamma-ray emission (the right panel of Fig. 8) by both leptonic (IC) and hadronic (p-p) models for the correspondingly derived parameters of CRs. The question is whether the observed microwave spectrum from the FBs is also compatible with the leptonic or hadron model.

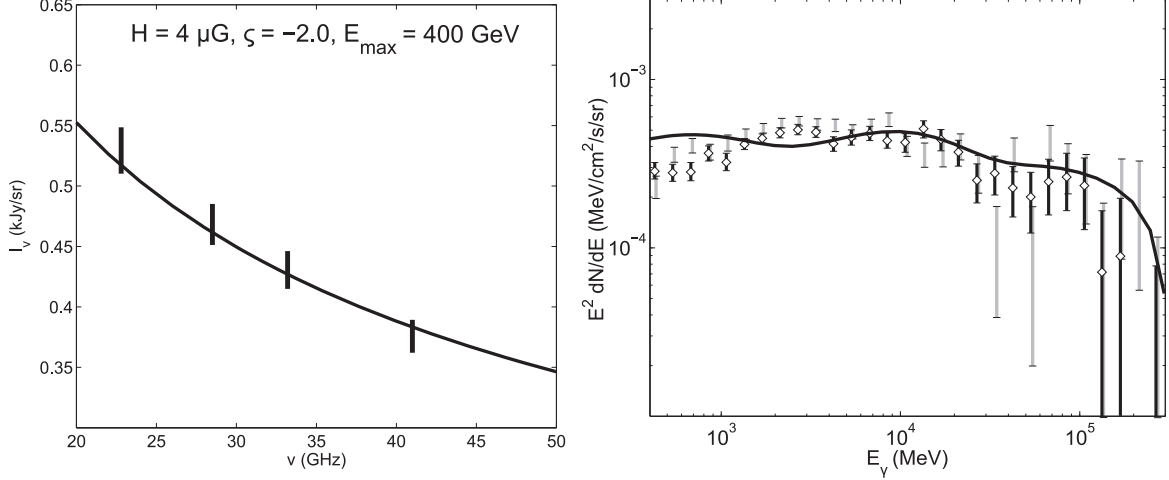


Figure 8. Spectrum of radio (left) and gamma-ray (right) emission from the FBs (see Cheng et al. 2014). The microwave data was taken from Planck Collaboration (2013), and gamma-ray from Ackermann et al. (2012, 2014). Figure adapted from Cheng et al. (2014) with permission.

7.2. Microwave origin in cosmic ray electron model

The origin of the microwave (see left panel of Fig. 8) was analysed for leptonic and hadronic models (see Ackermann et al. 2014), and the goal is to fit the gamma-ray and microwave observations within the same model.

The electron in the IC scenario should also produce the observed WMAP and Planck microwave spectrum and flux. Their properties can be derived from the observed density of gamma-ray produced by relativistic electrons that interact with the low-energy interstellar photons in the IC scenario for a magnetic field in the FBs in the range between 5 μG and 20 μG (see Ackermann et al. 2014). The best-fit magnetic field is about 8.4 μG . The synchrotron flux of the FBs from these electrons can be estimated as (see Ginzburg & Syrovatskii 1964, 1965),

$$\Phi_\nu \simeq 4\pi \frac{\sqrt{3}e^3}{m_e c^2} \int_{r_{\min}}^{r_0} B(r) r^2 dr \times \int \frac{\nu}{\nu_c} N_e(E) dE \int_{\nu/\nu_c}^{\infty} K_{5/3}(\eta) d\eta, \quad (58)$$

where $K_\mu(\eta)$ is the McDonald function, and

$$\nu_c(r, E) = \frac{3eB(r)}{4\pi m_e c} \left(\frac{E}{m_e c^2} \right)^2. \quad (59)$$

$\Phi_\nu(\nu(E_e))$ can be estimated from the density of relativistic electrons $N_e(E_e)$ in the FB envelope as,

$$N_e(E_e) \simeq \frac{\chi}{V_0} \frac{\Phi_\nu(\nu(E_e))}{E_e}, \quad (60)$$

where the parameter χ is

$$\chi = \frac{3m_e^3 c^5 \nu_0}{e^4 B_0^2}. \quad (61)$$

Although the main contribution to the IC signal comes from electrons at energies > 100 GeV while the main contribution to the Planck frequencies comes from electrons between 10 \sim 30 GeV, they match each other in the IC model.

7.3. Microwave origin in cosmic ray proton model

In the pure hadronic model (see Ackermann et al. 2014; Cheng et al. 2015a), the FB synchrotron emission is produced by secondary electrons from collisions of primary protons.

The approximated equations for the spectrum of secondary electrons produced by p-p and knock-on (KO) collisions (pe and ee), can be written as (see, e.g., Hayakawa 1969; Ginzburg 1989)

$$N_{se}(E_e, r) = \tau_e \int_{\frac{m_p}{m_e} E_e}^{\infty} N_p(E_p, r) n_H v_p d\sigma_{pp}(E_p), \quad (62)$$

$$N_{ss}(E_e, r) = \tau_e \int_{\frac{m_p}{m_e} E_e}^{\infty} N_p(E_p, r) v_p n_H \frac{d\sigma_{KO}(E_p, E')}{dE'} dE_p, \quad (63)$$

where τ_e is an integral over the rate of electron energy losses

$$\tau_e \sim \int_{E_e}^{E_{\max}} \frac{dE_e}{(dE_e/dt)_i}. \quad (64)$$

Here $(dE_e/dt)_i$ can be determined by bremsstrahlung, ionization, synchrotron or particle escape.

The synchrotron emission of the secondary electron from the FB envelope can be calculated from Eq. (58).

The pure hadronic model is unable to reproduce both gamma-ray and radio fluxes from the FBs at the same time. The problem is that the secondary electrons and positrons in the hadronic scenario produce synchrotron

radiation with a spectrum that is too soft compared to the microwave haze spectrum, whereas the overall normalization of the synchrotron radiation from the secondary particles is at least a factor of three to four smaller than the microwave level that a hadronic model requires (see [Cheng et al. 2015a](#)).

Thus, we conclude that a purely hadronic origin of the nonthermal emission (gamma and radio) from the FBs is problematic.

8. NUMBER OF RELATIVISTIC ELECTRONS IN THE FERMI BUBBLE ENVELOPE

The origin of relativistic electrons in the FB envelope is an open question. It was assumed that the FB envelopes might be bounded by a shock with the velocity $v_{\text{sh}} \sim 10^8 \text{ cm s}^{-1}$ (see, e.g., [Cheng et al. 2011](#); [Dorfi & Breitschwerdt 2012](#); [Peretti et al. 2022](#)). It was proposed that these CRs are accelerated at the shock by the standard mechanism of shock acceleration with the CR spectrum $Q(E_e) \propto E_e^{-2}$ (see, e.g. [Axford et al. 1977](#); [Krymskii 1977](#); [Bell 1978](#); [Blandford & Ostriker 1978](#)). However, the eROSITA (see [Predehl et al. 2020](#)) found that X-ray giant bubbles propagate with the velocity of the shock is about 340 km s^{-1} and its Mach number is only ≈ 1.5 , which does not correspond to an effective CR shock acceleration. Thus, CRs are not accelerated by a shock near the outer shell of eROSITA. Therefore, CRs should be produced by in-situ stochastic acceleration by MHD-turbulence W_k nearby the inner Bubble surface (see Section 6 the function W_k).

In the following, we focus on the in-situ stochastic (Fermi) acceleration of CRs by a hydromagnetic or super-sonic turbulence.

8.1. Electrons accelerated from background plasma in the Fermi Bubbles

In the model of [Cheng et al. \(2014\)](#), CR electrons can be directly accelerated from a background plasma. They suggested that the acceleration from the background plasma is able to explain the origin of the nonthermal particles responsible for producing the observed fluxes of radio and gamma-ray emissions from the bubbles.

The kinetic equation for the distribution function of electrons, $F(p, t)$, in the case of in-situ acceleration is described as

$$\begin{aligned} & \frac{\partial F(p, t)}{\partial t} + \frac{F(p, t)}{\tau_{\text{esc}}} \\ &= \frac{1}{p^2} \frac{\partial}{\partial p} p^2 \left[- \left(\frac{dp}{dt} \right)_C F(p, t) \right. \\ & \quad \left. + \{D_C(p) + D_F(p)\} \frac{\partial F(p, t)}{\partial p} \right]. \end{aligned} \quad (65)$$

The distribution function includes the thermal and non-thermal components of the particle distribution. Coefficient $(dp/dt)_C$ describes particle ionization/Coulomb

energy losses. $D_C(p)$ describes diffusion in the momentum space due to Coulomb collisions (for detail see [Lifshitz & Pitaevskii 1981](#)). The stochastic (Fermi) acceleration is described as diffusion in the momentum space with the diffusion coefficient $D_F(p)$. τ_{esc} is the lifetime of particles in the region of acceleration, e.g., due to escape from the region.

In an ionized plasma, the equilibrium (Maxwellian) spectrum of background charged particles is formed by Coulomb collisions. For the case of CR acceleration, there is a boundary, $E = E_{\text{inj}}$ between the equilibrium Maxwellian distribution and a power-law nonthermal spectrum of accelerated particles,

$$\frac{dE}{dt} = \alpha_0 E - \nu_0 E \left(\frac{kT}{E} \right)^{3/2}. \quad (66)$$

The energy of injection is

$$E_{\text{inj}} \sim kT \left(\frac{\nu_0}{\alpha_0} \right)^{2/3}. \quad (67)$$

Here the parameters α_0 and ν_0 are the acceleration and the ionization loss (by Coulomb collisions), respectively.

Making use of Eq. (65), [Gurevich \(1960\)](#) studied the process of the formal connection between equilibrium Maxwellian distribution of background particles and a power-law non-equilibrium spectrum of accelerated particles.

For slow time variations, the run-away flux of particles from the region of thermal Maxwellian distribution into the acceleration range is (see, e.g., [Dogiel 2000](#))

$$S_\zeta = S_0(t) \sqrt{\frac{2}{\pi}} \int_0^\zeta \zeta^2 \exp\left(-\frac{\zeta^2}{2}\right) d\zeta, \quad (68)$$

where $\zeta = p/p_0$ is the normalised momentum, and

$$S_0(t) = \sqrt{\frac{2}{\pi}} n(t) \exp\left(-\int_0^\infty \frac{\zeta d\zeta}{(1 + \alpha_0 \zeta^5 / \nu_0)}\right), \quad (69)$$

and $n(t)$ is the slow variation of the gas density.

In a non-equilibrium case this process forms an escape flux of runaway particles for energy $E > E_{\text{inj}}$. On the other hand, this process also forms an excess density at energies below $E \lesssim E_{\text{inj}}$, which distorts the thermal Maxwellian distribution. This can be interpreted as a ‘‘second’’ effective temperature higher than the gas equilibrium temperature.

This model of [Gurevich \(1960\)](#) has been applied to the processes of particle acceleration from background plasma in galaxy clusters (see [Dogiel 2000](#); [Liang et al. 2002](#); [Dogiel et al. 2007](#)), in the GC (see [Cheng et al. 2014](#)), and in the Galactic disk ([Dogiel et al. 2002](#)), in which excesses above thermal particles in X-ray range is expected.

For example, the spectrum of X-ray emission from the Galactic plane can be described as a multi-temperature

emission. Dogiel et al. (2002) interpreted this X-ray emission as the flux of runaway particles from background gas as a common effect of Coulomb collision (ionization losses) and stochastic acceleration (see Fig. 9). When compared with the spectrum of a simple combination of thermal and nonthermal gas, the spectrum with runaway flux is larger, in particular, in the transition range between the thermal and nonthermal part.

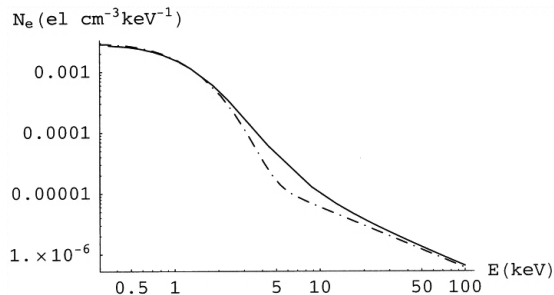


Figure 9. X-ray emission from the Galactic plane whose excess emission is above the equilibrium Maxwellian spectrum. Dash-dotted line is a simple combination of thermal plus nonthermal spectrum. Solid line is the spectrum with the effect of runaway flux. Figure reproduced from Dogiel et al. (2002) with permission.

The model of particle excess from background gas proposed for CRs by Dogiel (2000) was challenged by Petrosian (2001), Wolfe & Melia (2006) and Petrosian & East (2008). The problem was that the stochastic acceleration from a background plasma would (over) heat the plasma by the accelerated particles, because their energy would be quickly dumped into the thermal plasma by ionization losses. The energy, gained by the particles, is distributed to the whole plasma on a timescale much shorter than that of the acceleration process itself. As a result of the relatively inefficiency of bremsstrahlung for cooling the accelerated electrons, this tail is quickly dumped into the thermal body of the background plasma (plasma overheating without a prominent tail of accelerated particles). This effect prevents completely the formation of nonthermal spectra from background plasma.

However, Chernyshov et al. (2012) showed that the effect of overheating depends on the parameters of acceleration. It is insignificant if the stochastic acceleration is effective. This model depends on a value of p_{inj} and a free parameter of stochastic acceleration p_0 in the form of

$$D_F(p) = D_0 p^\zeta \theta(p - p_0), \quad (70)$$

where D_0 and ζ are constants. In general, p_{inj} is determined by $D_F(p_{\text{inj}}) = [p(dp/dt)_C]_{p_{\text{inj}}}$. In this model, the injection momentum is given by

$$D_0 p_{\text{inj}}^{(\zeta-1)} = \left[\left(\frac{dp}{dt} \right)_C \right]_{p_{\text{inj}}}. \quad (71)$$

For a high value of the acceleration momentum p_0 the runaway flux of thermal particles cools the plasma down from the very beginning. In spite of energy supply by external sources the plasma temperature drops down (analogue to Maxwell demon). Acceleration generates a prominent tail of accelerated particles but “excess” is not produced at the range around p_{inj} that was expected in Gurevich (1960), see Fig. 10. For $p_0 > p_{\text{inj}}$ plasma overheating is insignificant and stochastic acceleration works well. For $p_0 < p_{\text{inj}}$ plasma overheating is significant and stochastic acceleration is inhibited.

In any case, numerical calculations showed that the permitted parameters of the FB model are strongly restricted, and the model is unable to explain the observed fluxes of radio and gamma-ray emissions from the bubbles (see Cheng et al. 2014).

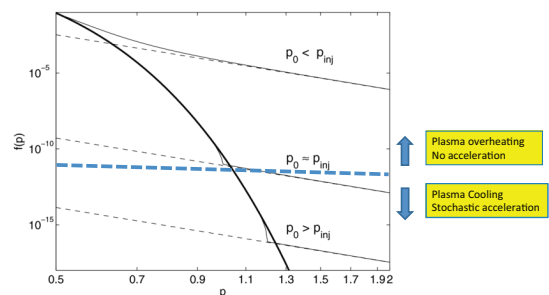


Figure 10. The spectrum of electrons accelerated from background plasma (see Chernyshov et al. 2012). The solid line is the density of electrons, $f(p)$. The thick solid line is the pure thermal Maxwellian distribution. The dashed line is the power-law approximation of the nonthermal tail. For $p_0 > p_{\text{inj}}$, overheating is insignificant. Figure adapted from Chernyshov et al. (2012) with permission.

8.2. Cosmic ray electrons re-accelerated in the Fermi Bubbles

CR electrons can be generated by sources in the Galactic disk (e.g., supernova remnant shocks, SNR shocks). Due to synchrotron, inverse Compton and adiabatic losses in the halo, Cheng et al. (2015b) deemed that these CR electrons with energies above several GeV are unable to reach the height of the FB envelope (which is about $8 \sim 10$ kpc). With appropriate parameters in the FB envelope, these electrons can be re-accelerated in-situ up to energies about 10^{12} eV, which is needed to reproduce the observed radio and gamma-ray emissions from the FBs and supply the required power.

The steady state kinetic equation for the relativistic electrons in FBs can be described in the form (see Cheng et al. 2015b)

$$Q(p)\delta(z) = -\nabla \cdot [D_s \nabla F - \mathbf{v}F] + \frac{1}{p^2} \frac{\partial}{\partial p} p^2 \left[\left(\frac{dp}{dt} - \frac{\nabla \cdot \mathbf{v}}{3} p \right) F - D_p \frac{\partial F}{\partial p} \right] \quad (72)$$

where $F(p, r, z)$ is the particle distribution function, $Q(p, r) \propto p^{-\gamma}$ is the source function of electrons in the Galactic disk ($z = 0$), $dp/dt = \mu E^2$ is the rate of synchrotron and inverse Compton energy losses, $D_s(p, r, z)$ is the coefficient of spatial diffusion, and $D_p(p, r, z) = \kappa p^2$ is the coefficient of momentum diffusion (coefficient of the Fermi re-acceleration), and $\mathbf{v}(r, z) = v_z \hat{e}_z = 3v'z\hat{e}_z$ ($v' = dv_z/dz$) is the wind velocity of advection in the halo in the z direction. The effect of the wind advection leads to adiabatic losses of CRs, $dp/dt = -p\nabla \cdot \mathbf{v}/3$. Consequently, the spectrum of electrons in the FBs in the acceleration region is harder than the case without advection.

Cheng et al. (2015b) showed that the gamma-ray and radio emissions of the re-accelerated electrons reproduced nicely the Fermi-LAT and Planck data points for the parameters: the spatial diffusion coefficient $D_s = 10^{29} \text{ cm}^2 \text{ s}^{-1}$, the energy loss rate $\nu = 2 \times 10^{-16} \text{ s}^{-1} \text{ GeV}^{-1}$, the velocity gradient of the advection in the halo $v' = 10^{-15} \text{ s}^{-1}$, the magnetic field strength is $B = 3 \mu\text{G}$, the thickness of the re-acceleration region (say, the FB envelope) is about $\Delta r_{\text{FB}} = 60 \text{ pc}$, and the parameter of re-acceleration in the FBs is $\kappa = 2 \times 10^{-14} \text{ s}^{-1}$.

The total power $\dot{\mathcal{E}}$ supplied by sources of Fermi re-acceleration in the FBs to produce high-energy electrons is needed

$$\dot{\mathcal{E}} = - \int_0^\infty 4\pi E \frac{\partial}{\partial p} \left(p^2 D_p \frac{\partial F}{\partial p} \right) dp, \quad (73)$$

where p and E are the particle momentum and particle kinetic energy, respectively.

To define the spectrum of accelerated electrons we estimated the number of GeV electrons that can reach an altitude of several kpc when the effect of advection $v(z)$ is essential in the Galactic halo (see Breitschwerdt et al. 1991; Bloemen et al. 1993; Breitschwerdt et al. 2002; Blasi et al. 2012). The spectrum of re-accelerated SNR electrons in the FBs is shown in Fig. 11 (cf. Cheng et al. 2015b). In the figure, the thick solid line is the spectrum of CR electrons from their sources in the Galactic disk (see, e.g., Berezhinsky et al. 1990). When re-acceleration (stochastic acceleration) and adiabatic losses are taken into account, the spectrum of electrons (thin dashed line) becomes harder than that of spectrum emitted by sources (thick solid line), but softer than the spectrum of pure re-acceleration (thin dash-dotted line). The spectrum for a velocity gradient $v' = 10^{-15} \text{ s}^{-1}$ (see, e.g., Bloemen et al. 1993; Breitschwerdt et al. 2002) is consistent with the observed one (dashed line in Fig. 11).

The model of re-acceleration within the envelope coincides nicely with the observed microwave and gamma-ray emissions shown in the left and right panels of Fig. 8, respectively.

In the phenomenological model, the power, $\dot{\mathcal{E}}$, is estimated numerically from the observed FB gamma-ray and microwave fluxes, and it is about $\dot{\mathcal{E}} \sim 2 \times 10^{38} \text{ erg s}^{-1}$. The density of high-energy electrons needed for the

observed gamma-ray flux is shown by the shaded gray region in Fig. 11.

With appropriate parameters these electrons can be re-accelerated up to an energy of 10^{12} eV , which explains in this model the origin of the observed gamma-ray and radio emissions from the FBs. However, although the model gamma-ray spectrum is consistent with the Fermi results, the model radio spectrum in the pure diffusion model is steeper than that observed by WMAP and Planck.

If adiabatic losses due to plasma outflows from the Galactic central regions are taken into account, we expect that the spectrum of electrons in the acceleration region will be harder than the one without advection. Our calculations with divergent outflows show that the gamma-ray and radio emissions by the re-accelerated electrons nicely reproduce the Fermi-LAT and the Planck data (see Fig. 8).

In essence, both gamma-ray and microwave observations can be explained by only one source of high energy electrons. The basic idea is summarized as follows. CR electrons from SNR in the Galactic disk are re-accelerated in the FB via supersonic turbulence (or multiple shocks). The resulting spectrum is hard, and in the high energy region the density of electrons exceeds the one to produce the observed gamma-ray emission. With adiabatic loss by the divergent flow, the density reduces but the spectrum is still hard enough to produce the observed microwave emission. Inevitably, some delicate balance or fine-tuning of parameters is needed.

9. COSMIC RAY PROTONS ESCAPING FROM THE FERMI BUBBLES INTO THE GALAXY

The fundamental question of the sources of CRs in the galaxy is still open. We present a number of models which may interpret the origin of CRs escaping from the FBs into the Galactic disk. The effect can be observed from the spectrum of CRs near Earth.

As described in Berezhinsky et al. (1990), the classical model of CR origin in the Galaxy is CRs are generated by SNRs in the Galactic disk with energies below 10^{15} eV . They escape into the Galactic halo with an effective spatial diffusion coefficient about $D_G = D_*(E/4 \text{ GeV})^{0.6}$ ($D_* = 6.2 \times 10^{28} \text{ cm}^2 \text{ s}^{-1}$), which is estimated from the observed chemical composition of CRs (for a modern nonlinear model of CR see Dogiel et al. 2020, and references therein). Plane shock acceleration produces a CR spectrum $F(E) \propto E^{-2}$ (see, e.g., Axford et al. 1977; Krymskii 1977; Bell 1978; Blandford & Ostriker 1978). The actual CR spectrum observed outside the acceleration region is a result of the process of acceleration in the region together with the process of particle leakage or escape from the region. Furthermore, the maximum energy that can be attained by CR particles depends on the size and/or lifetime of the acceleration region. Suppose v_{sh} is the shock velocity, and D_{sh} is the spatial diffusion coefficient in the

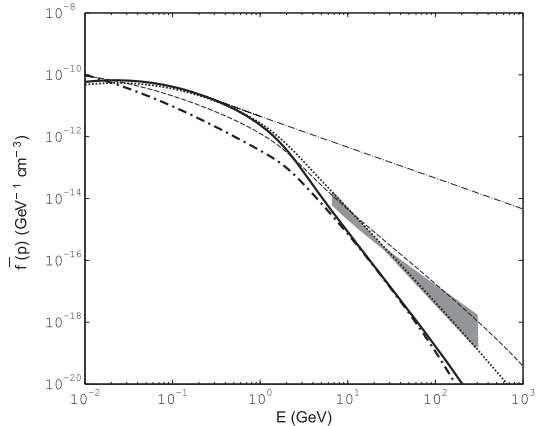


Figure 11. The spectrum of SNR electrons from the Galactic disk that have been re-accelerated in the FBs. The five spectra in the figure correspond to different cases of the model: (1) thick solid line: without re-acceleration, escape and advection; (2) thick dash-dotted line: without re-acceleration and escape but with advection; (3) thin dash-dotted line: with re-acceleration but without escape from the region and advection; (4) thin dotted line: with re-acceleration and escape from the region but without advection; (5) thin dashed line: with re-acceleration and advection but without escape. The density of electrons needed for the observed gamma-ray flux from the bubbles is shown by the gray region. The electron spectrum of case (5) can reproduce the gamma-ray data from Fermi-LAT and the microwave data from Planck (Fig. 8). The parameters of case (5) can be found in the main text. For parameters of other cases, the reader is referred to Cheng et al. (2015b). Figure reproduced from Cheng et al. (2015b) with permission.

shock vicinity. The minimum value of D_{sh} follows the Bohm’s limit, $D_{\text{sh}} \approx u r_L / 3$ (where $u \approx c$ is the speed of CR particles). The maximum energy is constrained by the size of the acceleration region becomes smaller than the diffusion length scale of the particles $l_D \sim D_{\text{sh}} / v_{\text{sh}}$, and/or the lifetime of the region is smaller than the acceleration time scale of the particles $\tau_{\text{acc}} \sim D_{\text{sh}} / v_{\text{sh}}^2$.

The observed CR spectrum (above 1 GeV) at Earth can be described as a broken power law, see the classic spectrum in Swordy (2001) (or Fig. 12 which shows the part above 10^{13} eV). The power law index is -2.7 between 10^9 and 10^{15} eV, and -3.1 between 10^{15} and several 10^{18} eV. Energy around 10^{15} eV is called the ‘knee’, where the spectrum changes from a harder one to a softer one. The spectrum beyond several 10^{18} eV becomes harder again and this region is called the ‘ankle’. The apparent cutoff at somewhat less than 10^{20} eV is commonly attributed to the Greisen-Zatsepin-Kuzmin limit due to the interaction of ultra high energy CRs with cosmic microwave background (Greisen 1966; Zatsepin & Kuz’min 1966). At energy smaller than 1 GeV, the spectrum is heavily affected by solar modu-

lation and activity of the Sun. Although the spectrum is a broken power law, the ‘joints’ (say the ‘knee’ and the ‘ankle’) are smooth. The origins of different parts of the spectrum should be somehow related (e.g., Axford 1994).

SNR shocks are believed to be the source of CRs (e.g., Berezhinsky et al. 1990). They can produce the spectral index -2.7 reasonably well. With the magnetic field around the SNR comparable the general interstellar field, Lagage & Cesarsky (1983) and Berezhko & Völk (2000) estimated the maximum energy of protons from SNRs is about $10^{13} \sim 10^{14}$ eV. However, with instabilities caused by cosmic ray streaming (e.g., non-resonant hybrid instability), Bell (2004) and Bykov et al. (2009) found that the fluctuated magnetic field can be orders of magnitude larger at the SNR shock (and so $D_{\text{sh}} \ll D_G$). The confinement time of CRs is longer and they can be accelerated up to 10^{15} eV (see also Bell 2013).

The SNR shock framework is able to describe the spectrum in the energy range $E < 10^{15}$ eV (see Fig. 12). However, for $E > 10^{15}$ eV, we need some other ideas (see, e.g., Bykov & Toptygin 1993). Larger and longer lifetime shocks are required, such as superbubbles (FB is an example). and strong galactic winds (e.g., Jokipii & Morfill 1985; Völk & Zirakashvili 2004; Cheng et al. 2012; Dorfi & Breitschwerdt 2012; Peretti et al. 2022; Zirakashvili et al. 2024). In the following, we analyze the spectrum of CRs accelerated in the FBs and discuss whether the bubble’s contribution may explain the ‘knee’ steepening. The idea is based on acceleration by multiple shocks. In a multiple-shock system, two length scales are important: (1) the average separation between two shocks $l_{\text{sh}} \sim v_{\text{sh}} \tau_c$ (where τ_c is the average time between the creation of two consecutive shocks), and (2) the diffusion length scale at the shock $l_D (\sim D_{\text{sh}} / v_{\text{sh}})$. We will focus on the regime $l_{\text{sh}} \ll l_D$ (the supersonic turbulence regime), for energies beyond the ‘knee’ ($E > 10^{15}$ eV).

An illustration of a possible multiple-shock structure in the FBs is shown in Fig. 13.

9.1. Escape of cosmic ray protons re-accelerated by supersonic turbulence inside the Fermi Bubbles

Cheng et al. (2012) suggested an alternative model of CRs in the FBs (see also Cheng et al. 2006, 2007; Dogiel et al. 2009a,b,c). They assumed that up to several hundred TDEs might have occurred in the past 10 Myr. This would have generated a series of shocks propagating through the central part of the Galactic halo, which would produce relativistic CRs via multiple-shock acceleration. The average separation between two shocks is then

$$l_{\text{sh}} = v_{\text{sh}} \tau_{\text{cap}} \simeq 30 \left(\frac{\tau_{\text{cap}}}{3 \times 10^4 \text{ yr}} \right) \left(\frac{v_{\text{sh}}}{10^8 \text{ cm s}^{-1}} \right) \text{ pc}, \quad (74)$$

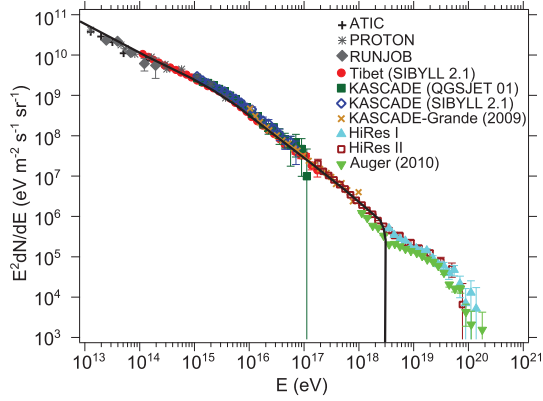


Figure 12. CR spectrum at the Earth as a combination of the contributions from the SNRs in the Galactic disk and the stochastic acceleration in the FBs. Figure reproduced from Cheng et al. (2012) with permission.

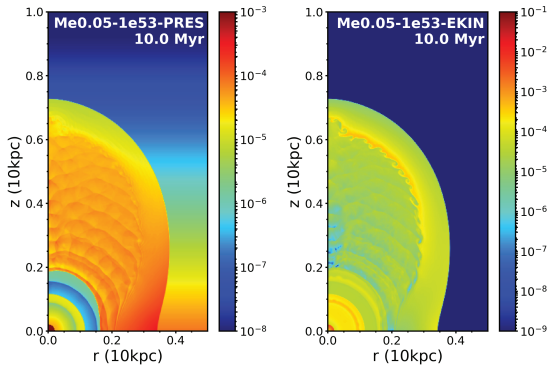


Figure 13. A possible multiple-shock structure in the FBs resulting from multiple TDEs at the GC. The figure shows the pressure (left panel) and kinetic energy (right panel) distributions of a numerical simulation of the FBs in an exponential halo. In the panels, “Me0.05-1e53” corresponds to multiple TDEs with 0.05 Myr between successive TDE and the energy release by TDE is 10^{53} erg. The simulation ends at 10.0 Myr. The unit of the color bar in both panels is 1.178×10^{-8} erg cm^{-3} .

where τ_{cap} is the average time between two stellar captures by the SMBH.

We apply the model of Bykov & Fleishman (1992) and Bykov & Toptygin (1993) for CRs acceleration by multiple shocks in the FBs. Under the conditions of supersonic turbulence (multiple-shock structure) the regime of acceleration is characterized by $l_{\text{sh}} \ll l_{\text{D}}$.

The steady state kinetic equation in axisymmetric geometry is

$$\frac{\partial}{\partial z} \left[D_s(p, r) \frac{\partial F}{\partial z} \right] + \frac{1}{r} \frac{\partial}{\partial r} \left[D_s(p, r) r \frac{\partial F}{\partial r} \right] + \frac{1}{p^2} \frac{\partial}{\partial p} \left[D_p(p, r) p^2 \frac{\partial F}{\partial p} \right] = -Q(p, r, z). \quad (75)$$

The spatial diffusion coefficient inside and outside the bubble is,

$$D_s(p, r) = D_B \theta(r_B - r) + D_G \theta(r - r_B), \quad (76)$$

where r_B is the radius of the bubbles. Inside the bubbles, as a result of interaction with supersonic turbulence $D_s = D_B \approx ul_{\text{sh}}/3 \approx cl_{\text{sh}}/3$. Outside the bubbles, $D_s = D_G$, is the average diffusion coefficient in the Galaxy, e.g., the one described in Berezhinsky et al. (1990). The momentum diffusion coefficient is nonzero inside the bubbles only,

$$D_p(p, r) = \kappa_B p^2 \theta(r_B - r), \quad (77)$$

and $\kappa_B \sim v_{\text{sh}}^2/D_B$. The parameters in the FBs can be estimated numerically from the observed CR spectrum.

Using the method of separation variables as in Bulanov et al. (1972) and Bulanov & Dogel (1974) to solve Equation (75) for the spectrum of CRs, generated by SNRs with the standard model of CR propagation and escape in the Galactic halo (see, e.g., Ginzburg & Syrovatskii 1964; Berezhinsky et al. 1990; Strong et al. 2007). This model describes the observed CR spectrum near Earth in the range below the ‘knee’, 10^{15} eV (see Figure 12).

Cheng et al. (2012) interpreted the CR spectrum near Earth in the energy range from 10^{15} eV to a few 10^{18} eV (from the ‘knee’ to the ‘ankle’) as a combined result of acceleration in the FB and escape. The acceleration is provided by the supersonic turbulence in the FB (see Bykov & Toptygin 1993). Under the set of parameters in Cheng et al. (2012), the ratio of the escape time to the acceleration time is about 1.9.

In order to derive the CR spectrum near Earth, Cheng et al. (2012) matched the solutions for the spectra inside the FB and outside (in the halo) at $r = r_B$ (see Equations (75) and (76)). Basically, the model can reproduce the CR spectrum from 10^{13} eV to several 10^{18} eV. However, we should point out that the numerical result described here (Cheng et al. 2012) has free parameters and some physics have been ignored (e.g., adiabatic loss), and the result might not be very solid. It is imperative to have further investigations.

A brief summary of the idea is as follows. CRs from SNR ($< 10^{15}$ eV) are re-accelerated in the FB by multiple shocks or supersonic turbulence. As the shocks are larger and live longer in FB, CRs can be accelerated to much higher energies (up to 10^{19} eV). Acceleration by multiple shocks inside the bubbles gives a harder spectrum, hence the contribution of the FB to CRs within the ‘knee’ ($< 10^{15}$ eV) is subordinate to SNR). The high energy CRs escaping from the bubbles constitute the sole source of CRs in the range between the ‘knee’ to the ‘ankle’ (10^{15} to several 10^{18} eV) observed at Earth. In the model, some fine-tuning of parameters is inevitable.

Here we present a brief summary of our perspective of the Fermi Bubbles at the Galactic Centre.

- The key point of the bubbles is a huge energy release of $10^{55} \sim 10^{56}$ erg in the Galactic centre whose origin is still unknown yet.
- We assume that the energy source of the bubbles could be a routine tidal disruption of stars near the central supermassive black hole. Each disruption of a star releases a total energy about $10^{52} \sim 10^{53}$ erg. For a typical rate of stellar capture (once 10^4 years), this can provide a luminosity $\gtrsim 10^{41}$ erg s^{-1} from the Galactic Centre. These processes of stellar tidal disruption events can be directly observed in some external galaxies.
- Hydrodynamic models can describe the envelope of bubble propagation in the Galactic halo where the gas distribution is nonuniform. The distribution is commonly characterized by an exponential or a power-law function. The observed shape of the Fermi bubbles seems to suggest an exponential halo. If the velocity of the top of the envelope prevails the sound velocity in the halo, then the envelope may reach the size of 10 kpc.
- The surface of the top of the envelope propagates with acceleration in the halo. As a result, Rayleigh-Taylor instabilities are developed and they will destroy the bubble envelope at the top. We expect excitation of hydrodynamic instabilities and generation of a hydrodynamic turbulence there.
- Turbulent motions act as a source of waves, which are manifested as a hierarchy of eddies, and act as a direct source of energy to the MHD waves (via the Lighthill mechanism). For small Mach numbers, a small fraction of the power radiated by the turbulent motion is Alfvén waves.
- The coefficients of the spatial and momentum diffusion of the system of nonlinear kinetic equations of the cosmic ray distribution function are derived from the spectrum of MHD waves. These coefficients were calculated analytically, but we were unable to estimate the numerical values for the

bubbles because of the lack of available observation on the wave spectrum.

- We estimated roughly the spatial and momentum diffusions of cosmic rays in the envelope from the data of gamma-ray and microwave radiations from the Fermi bubbles.
- We concluded that the observed gamma-ray and microwave radiations from the envelope of the Fermi Bubbles are generated by cosmic ray electrons only. Contribution of cosmic ray protons can be neglected.
- We prefer the model that GeV cosmic ray electrons from supernova remnants in the Galactic disk are re-accelerated in situ in the bubbles to TeV energy range. With the help of a divergent flow, this can reproduce the data of both gamma-ray and microwave observations.
- On the other hand, high energy cosmic ray protons can escape the bubbles and reach the Earth. Cosmic ray protons from supernova remnants can be accelerated in the bubbles by supersonic turbulence to higher energies. We found that the escape high energy protons that arrive the Earth can reproduce the spectrum and flux of cosmic rays in the range $10^{15} \sim 10^{18}$ eV (from the ‘knee’ to the ‘ankle’) observed near Earth.

Acknowledgements

First of all, let us thank colleagues who participated as co-authors of publications, mentioned in the list of references. It was a great joy for us to collaborate with them, and a significant contribution for this review we got from their collaboration.

All of them we thank very much and keep memory about any of you.

We are grateful for the nice atmosphere where we spent time participating in seminars and private talks with our colleagues from: P. N. Lebedev Institute of Physics (Russia), National Central University (Taiwan), The University of Hong Kong (Hong Kong), Max-Planck-Institut für Extraterrestrische Physik (Germany), Institute of Space and Astronautical Science (Japan), University of Bristol (UK), etc.

We are grateful to the International Space Science Institute (ISSI(Bern) and ISSI-BJ (Beijing)) which organized several workshops, whose informal and warm atmosphere helped us to understand some problems on Fermi Bubbles origin.

REFERENCES

- Ackermann, M., Ajello, M., Atwood, W. B. et al. 2012, “Fermi-LAT Observations of the Diffuse γ -Ray Emission: Implications for Cosmic Rays and the Interstellar Medium”, *ApJ*, 750, 3
- Ackermann, M., Albert, A., Atwood, W. B. et al. 2014, “The Spectrum and Morphology of the Fermi Bubbles”, *ApJ*, 793, 64

- Axford, W. I., Leer E., & Skadron, G. 1977, “The Acceleration of Cosmic Rays by Shock Waves”, in *Proceedings of the 15th International Cosmic Ray Conference*, 15th ICRC, Plovdiv, Bulgaria, 13-26 August 1977; 11, 132-137
- Axford, W. I. 1994, “The Origins of High-Energy Cosmic Rays”, *ApJS*, 90, 937-944
- Baumgartner, V., & Breitschwerdt, D. 2013, “Superbubble evolution in disk galaxies. I. Study of blow-out by analytical models”, *A&A*, 557, A140
- Bell, A. R. 1978, “The acceleration of cosmic rays in shock fronts - I”, *MNRAS*, 182, 147-156
- Bell, A. R. 2004, “Turbulent amplification of magnetic field and diffusive shock acceleration of cosmic rays”, *MNRAS*, 353, 550-558
- Bell, A. R. 2013, “Cosmic ray acceleration”, *Astropart. Phys.*, 43, 56-70
- Berezhko, E. G., & Völk, H. J. 2000, “Kinetic theory of cosmic ray and gamma-ray production in supernova remnants expanding into wind bubbles”, *A&A*, 357, 283-300
- Berezinskii, V. S., Bulanov, S. V., Dogiel, V. A., Ginzburg, V. L., & Ptuskin, V. S. 1990, *Astrophysics of Cosmic Rays*, ed. V. L. Ginzburg; North Holland: Amsterdam
- Bisnovatyi-Kogan, G. S., & Silich, S. A. 1995, “Shock-wave propagation in the nonuniform interstellar medium”, *RvMP*, 67, 661-712
- Bland-Hawthorn, J., & Cohen, M. 2003, “The Large-Scale Bipolar Wind in the Galactic Center”, *ApJ*, 582, 246-256
- Blandford, R. D., & Ostriker, J. P. 1978, “Particle acceleration by astrophysical shocks”, *ApJ*, 221, L29-L32
- Blasi, P. 2000, “Stochastic Acceleration and Nonthermal Radiation in Clusters of Galaxies”, *ApJ*, 532, L9-L12
- Blasi, P., Amato, E., & Serpico, P. D. 2012, “Spectral Breaks as a Signature of Cosmic Ray Induced Turbulence in the Galaxy”, *PRL*, 109, 061101
- Bloemen, J. B. G. M., Dogiel, V. A., Dorman, V. L., & Ptuskin, V. S. 1993, “Galactic diffusion and wind models of cosmic-ray transport. I. Insight from CR composition studies and gamma-ray observations”, *A&A*, 267, 372-387
- Breitschwerdt, D., McKenzie, J. F., & Völk, H. J. 1991, “Galactic winds. I. Cosmic ray and wave-driven winds from the galaxy”, *A&A*, 245, 79-98
- Breitschwerdt, D., Dogiel, V. A., & Völk, H. J. 2002, “The gradient of diffuse γ -ray emission in the Galaxy”, *A&A*, 385, 216-238
- Brunetti, G., Setti, G., Feretti, L., & Giovannini, G. 2001, “Particle reacceleration in the Coma cluster: radio properties and hard X-ray emission”, *MNRAS*, 320, 365-378
- Brunetti, G., Blasi, P., Cassano, R., & Gabici, S. 2004, “Alfvénic reacceleration of relativistic particles in galaxy clusters: MHD waves, leptons and hadrons”, *MNRAS*, 350, 1174-1194
- Brunetti, G., & Blasi, P. 2005, “Alfvénic reacceleration of relativistic particles in galaxy clusters in the presence of secondary electrons and positrons”, *MNRAS*, 363, 1173-1187
- Bulanov, S. V., Dogel', V. A., & Syrovatskij, S. I. 1972, “The Electron Component of Cosmic Rays. I. Spatial Distribution and Energy Spectrum”, *Cosmic Res.*, 10, 478
- Bulanov, S. V., & Dogel, V. A. 1974, “The Influence of the Energy Dependence of the Diffusion Coefficient on the Spectrum of the Electron Component of Cosmic Rays and the Radio Background Radiation of the Galaxy”, *Ap&SS*, 29, 305-318
- Burrows, D. N., Kennea, J. A., Ghisellini, G. et al. 2011, “Relativistic jet activity from the tidal disruption of a star by a massive black hole”, *Nature*, 476, 421-424
- Bykov, A. M., & Fleishman, G. D. 1992, “On non-thermal particle generation in superbubbles”, *MNRAS*, 255, 269-275
- Bykov, A. M., & Toptygin, I. N. 1993, “Particle kinetics in highly turbulent plasmas (renormalization and self-consistent field methods)”, *Phys. Usp.*, 36, 1020-1052
- Bykov, A. M., Osipov, S. M., & Toptygin, I. N. 2009, “Long-wavelength MHD instability in the prefront of collisionless shocks with accelerated particles”, *Astron. Lett.*, 35, 555-563
- Chandrasekhar, S. 1961, *Hydrodynamic and Hydromagnetic Stability*, International Series of Monographs on Physics, Oxford University Press: Oxford
- Cheng, K.-S., Chernyshov, D. O., & Dogiel, V. A. 2006, “Annihilation Emission from the Galactic Black Hole”, *ApJ*, 645, 1138-1151
- Cheng, K.-S., Chernyshov, D. O., & Dogiel, V. A. 2007, “Diffuse gamma-ray emission from the Galactic center – a multiple energy injection model”, *A&A*, 473, 351-356
- Cheng, K.-S., Chernyshov, D. O., Dogiel, V. A., Ko, C. M., & Ip, W.-H. 2011, “Origin of the Fermi Bubble”, *ApJL*, 731, L17
- Cheng, K.-S., Chernyshov, D. O., Dogiel, V. A., Ko, C. M., Ip, W.-H., & Wang, Y. 2012, “The Fermi Bubble as a Source of Cosmic Rays in the Energy Range $> 10^{15}$ eV”, *ApJ*, 746, 116
- Cheng, K.-S., Chernyshov, D. O., Dogiel, V. A., & Ko, C. M. 2014, “Multi-wavelength Emission from the Fermi Bubbles. I. Stochastic Acceleration from Background Plasma”, *ApJ*, 790, 23

- Cheng, K.-S., Chernyshov, D. O., Dogiel, V. A., & Ko, C. M. 2015a, “Multi-wavelength Emission from the Fermi Bubble. II. Secondary Electrons and the Hadronic Model of the Bubble”, *ApJ*, 799, 112
- Cheng, K.-S., Chernyshov, D. O., Dogiel, V. A., & Ko, C. M. 2015b, “Multi-wavelength Emission from the Fermi Bubble. III. Stochastic (Fermi) Re-acceleration of Relativistic Electrons Emitted by SNRs”, *ApJ*, 804, 135
- Cheng, K.-S., Chernyshov, D. O., Dogiel, V. A., Kong, A. K. H., & Ko, C. M. 2016, “X-Ray Afterglow of Swift J1644+57: A Compton Echo?”, *ApJL*, 816, L10
- Chernyshov, D. O., Dogiel, V. A., & Ko, C. M. 2012, “Stochastic Particle Acceleration and the Problem of Background Plasma Overheating”, *ApJ*, 759, 113
- Dai, L., McKinney, J. C., Roth, N. et al. 2018, “A Unified Model for Tidal Disruption Events”, *ApJL*, 859, L20
- Dai, L., Lodato, G., & Cheng, R. 2021, “The Physics of Accretion Discs, Winds and Jets in Tidal Disruption Events”, *SSRv*, 217, 12
- Dogiel, V. A. 2000, “On the thermal origin of the hard X-ray emission from the Coma cluster”, *A&A*, 357, 66-74
- Dogiel, V. A., Inoue, H., Masai, K., Schönfelder, V., & Strong, A. W. 2002, “The Origin of Diffuse X-Ray Emission from the Galactic Ridge. I. Energy Output of Particle Sources”, *ApJ*, 581, 1061-1070
- Dogiel, V. A., Colafrancesco, S., Ko, C. M., Kuo, P. H., Hwang, C. Y., Ip, W.-H., Birkinshaw, M., & Prokhorov, D. A. 2007, “In-situ acceleration of subrelativistic electrons in the Coma halo and the halo’s influence on the Sunyaev-Zeldovich effect”, *A&A*, 461, 433-443
- Dogiel, V. A., Cheng, K.-S., Chernyshov, D. et al. 2009a, “Origin of 6.4 keV Line Emission from Molecular Clouds in the Galactic Center”, *PASJ*, 61, 901
- Dogiel, V. A., Chernyshov, D., Yuasa, T. et al. 2009b, “Origin of Thermal and Non-Thermal Hard X-Ray Emission from the Galactic Center”, *PASJ*, 61, 1099-1105
- Dogiel, V. A., Tatischeff, V., Cheng, K.-S. et al. 2009c, “Nuclear interaction gamma-ray lines from the Galactic center region”, *A&A*, 508, 1-7
- Dogiel, V. A., Ivlev, A. V., Chernyshov, D. O., & Ko, C. M. 2020, “Formation of the Cosmic-Ray Halo: Galactic Spectrum of Primary Cosmic Rays”, *ApJ*, 903, 135
- Donato, D., Cenko, S. B., Covino, S. et al. 2014, “A Tidal Disruption Event in a nearby Galaxy Hosting an Intermediate Mass Black Hole”, *ApJ*, 781, 59
- Dorfi, E. A., & Breitschwerdt, D. 2012, “Time-dependent galactic winds. I. Structure and evolution of galactic outflows accompanied by cosmic ray acceleration”, *A&A*, 540, A77
- Eilek, J. A. 1979, “Particle reacceleration in radio galaxies”, *ApJ*, 230, 373-385
- Eilek, J. A., & Hendriksen, R. N. 1984, “The electron energy spectrum produced in radio sources by turbulent, resonant acceleration”, *ApJ*, 277, 820-831
- Fujita, Y., Takizawa, M., & Sarazin C. L. 2003, “Nonthermal Emissions from Particles Accelerated by Turbulence in Clusters of Galaxies”, *ApJ*, 584, 190-202
- Genzel, R., Eisenhauer, F., & Gillessen, S. 2010, “The Galactic Center massive black hole and nuclear star cluster”, *RvMP*, 82, 3121-3195
- Gezari, S. 2021, “Tidal Disruption Events”, *ARA&A*, 59, 21-58
- Ghez, A. M., Salim, S., Hornstein, S. D. et al. 2005, “Stellar Orbits around the Galactic Center Black Hole”, *ApJ*, 620, 744-757
- Gillessen, S., Eisenhauer, F., Trippe, S. et al. 2009, “Monitoring Stellar Orbits Around the Massive Black Hole in the Galactic Center”, *ApJ*, 692, 1075-1109
- Ginzburg, V. L., & Syrovatskii, S. I. 1964, *The Origin of Cosmic Rays*, Macmillan: New York
- Ginzburg, V. L., & Syrovatskii, S. I. 1965, “Cosmic Magnetobremstrahlung (Synchrotron Radiation)”, *ARA&A*, 3, 297-350
- Ginzburg, V. L. 1989, *Applications of Electrodynamics in Theoretical Physics and Astrophysics*, Gordon and Breach: New York
- Goodwin, A. J., Alexander, K. D., Miller-Jones, J. C. A. et al. 2023, “A radio-emitting outflow produced by the tidal disruption event AT2020vwl”, *MNRAS*, 522, 5084-5097
- Greisen, K. 1966, “End to the Cosmic-Ray Spectrum?”, *PRL*, 16, 748-750
- Gurevich, A. V. 1960, “On the amount of accelerated particles in an ionized gas under various accelerating mechanisms”, *Sov. Phys JETP*, 38, 1150-1157
- Hayakawa, S. 1969, *Cosmic Ray Physics*, Wiley-Interscience: New York
- Hendriksen, R. N., Bridle, A. H., & Chan, K. L. 1982, “Synchrotron brightness distribution of turbulent radio jets”, *ApJ*, 257, 63-74
- Heywood, I., Camilo, F., Cotton, W. D. et al. 2019, “Inflation of 430-parsec bipolar radio bubbles in the Galactic Centre by an energetic event”, *Nature*, 573, 235-237
- Hung, T., Gezari, S., Cenko, S. B. et al. 2018, “Sifting for Sapphires: Systematic Selection of Tidal Disruption Events in iPTF”, *ApJS*, 238, 15
- Jokipii, J. R., & Morfill, G. E. 1985, “On the origin of high-energy cosmic rays”, *ApJ*, 290, L1-L4

- Kahn, F. D. 1998, “The Galactic Fountain”, in *The Local Bubble and Beyond Lyman-Spitzer-Colloquium*, eds. D. Breitschwerdt, M. J. Freyberg, and J. Trümper, IAU Colloquium 166, Garching, Germany, 21-25 April 1997; Lecture Notes in Physics, Springer: Berlin; 506, 483-494
- Kamae, T., Karlsson, N., Mizuno, T. et al. 2006, “Parameterization of γ , e^\pm , and Neutrino Spectra Produced by p - p Interaction in Astronomical Environments”, *ApJ*, 647, 692-708
- Kara, E., Miller, J. M., Reynolds, C., & Dai, L. 2016, “Relativistic reverberation in the accretion flow of a tidal disruption event”, *Nature*, 535, 388-390
- Kato, S. 1968, “Generation of Alfvén Waves from Turbulence”, *PASJ*, 20, 59-72
- Ko, C. M., Breitschwerdt, D., Chernyshov, D. O., Cheng, H., Dai, L., & Dogiel, V. A. 2020, “Analytical and Numerical Studies of Central Galactic Outflows Powered by Tidal Disruption Events: A Model for the Fermi Bubbles?”, *ApJ*, 904, 46
- Kompaneets, A. S. 1960, “A point explosion in the uniform atmosphere”, *Akademiia Nauk SSSR, Doklady (DoSSR, in Russian)*, 130, 1001-1003
- Krymskii, G. F. 1977, “Mechanism of regular acceleration on the front of the shock wave”, *Akademiia Nauk SSSR Dokl. (DoSSR, in Russian)*, 234, 1306-1307
- Kulsrud, R. 1955, “Effect of Magnetic Fields on Generation of Noise by Isotropic Turbulence”, *ApJ*, 121, 461-480
- Lagage, P. O., & Cesarsky, C. J. 1983, “The maximum energy of cosmic rays accelerated by supernova shocks”, *A&A*, 125, 249-257
- Landau, L. D., & Lifshitz, E. M. 1987, *Fluid Mechanics*, Second Edition, Pergamon Press: Oxford
- Levan, A. J., Tanvir, N. R., Cenko, S. B. et al. 2011, “An Extremely Luminous Panchromatic Outburst from the Nucleus of a Distant Galaxy”, *Science*, 333, 199-202
- Liang, H., Dogiel, V. A., & Birkinshaw, M. 2002, “The origin of radio haloes and non-thermal emission in clusters of galaxies”, *MNRAS*, 337, 567-577
- Lifshitz, E. M., & Pitaevskii, L. P. 1981, *Physical Kinetics*, Pergamon Press: Oxford
- Lighthill, M. J. 1952, “On Sound Generated Aerodynamically. I. General Theory”, *Proc. Roy. Soc. London A*, 211, 564-587
- Lin, D., Guillochon, J., Komossa, S. et al. 2017, “A likely decade-long sustained tidal disruption event”, *Nat Astron*, 1, 0033
- Lu, W., & Kumar, P. 2018, “On the Missing Energy Puzzle of Tidal Disruption Events”, *ApJ*, 865, 128
- Mertsch, P., & Sarkar, S. 2011, “Fermi Gamma-Ray ‘Bubbles’ from Stochastic Acceleration of Electrons”, *PRL*, 107, 091101
- Metzger, B. D., & Stone, N. C. 2016, “A bright year for tidal disruptions”, *MNRAS*, 461, 948-966
- Miller, J. A., & Roberts, D. A. 1995, “Stochastic Proton Acceleration by Cascading Alfvén Waves in Impulsive Solar Flares”, *ApJ*, 452, 912-932
- Miller, M. J., & Bregman, J. N. 2016, “The Interaction of the Fermi Bubbles with the Milky Way’s Hot Gas Halo”, *ApJ*, 829, 9
- Mockler, B., & Ramirez-Ruiz, E. 2021, “An Energy Inventory of Tidal Disruption Events”, *ApJ*, 906, 101
- Moskalenko, I. V., & Strong, A. W. 1998, “Production and Propagation of Cosmic-Ray Positrons and Electrons”, *ApJ*, 493, 694-707
- Moskalenko, I. V., Porter, T. A., & Strong, A. W. 2006, “Attenuation of Very High Energy Gamma Rays by the Milky Way Interstellar Radiation Field”, *ApJ*, 640, L155-L158
- Mou, G., Wu, J., & Sofue, Y. 2023, “Cosmic-ray electrons and the magnetic field of the North Polar Spur”, *A&A*, 676, L3
- Nakashima, S., Koyama, K., Wang, Q. D. et al. 2019, “X-Ray Observation of a Magnetized Hot Gas Outflow in the Galactic Center Region”, *ApJ*, 875, 32
- Nayakshin, S., & Zubovas, K. 2018, “Sgr A* envelope explosion and the young stars in the centre of the Milky Way”, *MNRAS*, 478, L127-L131
- Norman, C. A., & Ferrara, A. 1996, “The Turbulent Interstellar Medium: Generalizing to a Scale-dependent Phase Continuum”, *ApJ*, 467, 280-291
- Parker, E. N. 1964, “A Mechanism for Magnetic Enhancement of Sound-Wave Generation and the Dynamical Origin of Spicules”, *ApJ*, 140, 1170-1173
- Peretti, E., Morlino, G., Blasi, P., & Cristofari, P. 2022, “Particle acceleration and multimessenger emission from starburst-driven galactic winds”, *MNRAS*, 511, 1336-1348
- Petrosian, V. 2001, “On the Nonthermal Emission and Acceleration of Electrons in Coma and Other Clusters of Galaxies”, *ApJ*, 557, 560-572
- Petrosian, V., & East, W. E. 2008, “Heating and Acceleration of Intracluster Medium Electrons by Turbulence”, *ApJ*, 682, 175-185
- Piran, T., Svirski, G., Krolik, J., Cheng, R. M., & Shiokawa, H. 2015, “Disk Formation Versus Disk Accretion—What Powers Tidal Disruption Events?”, *ApJ*, 806, 164

- Planck Collaboration 2013, “Planck intermediate results. IX. Detection of the Galactic haze with Planck”, *A&A*, 554, A139
- Ponti, G., Hofmann, F., Churazov, E. et al. 2019, “An X-ray chimney extending hundreds of parsecs above and below the Galactic Centre”, *Nature*, 567, 347-350
- Ponti, G., Morris, M. R., Churazov, E. et al. 2021, “The Galactic center chimneys: the base of the multiphase outflow of the Milky Way”, *A&A*, 646, A66
- Porter, T. A., Moskalenko, I. V., Strong, A. W. et al. 2008, “Inverse Compton Origin of the Hard X-Ray and Soft Gamma-Ray Emission from the Galactic Ridge”, *ApJ*, 682, 400-407
- Predehl, P., Sunyaev, R. A., Becker, W. et al. 2020, “Detection of large-scale X-ray bubbles in the Milky Way halo”, *Nature*, 588, 227-231
- Ptuskin, V. S., Moskalenko, I. V., Jones, F. C., Strong, A. W., & Zirakashvili, V. N. 2006, “Dissipation of Magnetohydrodynamic Waves on Energetic Particles: Impact on Interstellar Turbulence and Cosmic-Ray Transport”, *ApJ*, 642, 902-916
- Rees, M. J. 1988, “Tidal disruption of stars by black holes of $10^6 - 10^8$ solar masses in nearby galaxies”, *Nature*, 333, 523-528
- Sarkar, K. C., Mondal, S, Sharma, P., & Piran, T. 2023, “Misaligned Jets from Sgr A* and the Origin of Fermi/eROSITA Bubbles”, *ApJ*, 951, 36
- Sarkar, K. C. 2024, “The Fermi/eROSITA bubbles: a look into the nuclear outflow from the Milky Way”, *A&ARv*, 32, 1
- Schulreich, M., & Breitschwerdt, D. 2022, “The time-dependent Rayleigh-Taylor instability in interstellar shells and supershells, including the eROSITA bubbles”, *MNRAS*, 509, 716-737
- Sedov, L. I. 1959, *Similarity and Dimensional Methods in Mechanics*, Academic Press: New York
- Sofue, Y. 1977, “Propagation of magnetohydrodynamic waves from the galactic center. Origin of the 3-kpc arm and the North Polar Spur”, *A&A*, 60, 327-336
- Stein, R. F. 1981, “Stellar chromospheric and coronal heating by magnetohydrodynamic waves”, *ApJ*, 246, 966-971
- Stone, N. C., & Metzger, B. D. 2016, “Rates of stellar tidal disruption as probes of the supermassive black hole mass function”, *MNRAS*, 455, 859-883
- Strong, A. W., Moskalenko, I. V., & Ptuskin, V. S. 2007, “Cosmic-Ray Propagation and Interactions in the Galaxy”, *ARNPS*, 57, 285-327
- Su, M., Slatyer, T. R., & Finkbeiner, D. P. 2010, “Giant Gamma-ray Bubbles from Fermi-LAT: Active Galactic Nucleus Activity or Bipolar Galactic Wind?”, *ApJ*, 724, 1044-1082
- Swordy, S. 2001, “The Energy Spectra and Anisotropies of Cosmic Rays”, *SSRv*, 99, 85-94
- Vladimirov, A. E., Digel, S. W., Johannesson, G. et al. 2011, “GALPROP WebRun: An internet-based service for calculating galactic cosmic ray propagation and associated photon emissions”, *CoPhC*, 182, 1156-1161
- Völk, H. J., & Zirakashvili, V. N. 2004, “Cosmic ray acceleration by spiral shocks in the galactic wind”, *A&A*, 417, 807-817
- Wolfe, B., & Melia, F. 2006, “Covariant Kinetic Theory with an Application to the Coma Cluster”, *ApJ*, 638, 125-137
- Yang, H.-Y. K., Ruszkowski, M., Ricker, P. M., Zweibel, E., & Lee, D. 2012, “The Fermi Bubbles: Supersonic Active Galactic Nucleus Jets with Anisotropic Cosmic-Ray Diffusion”, *ApJ*, 761, 185
- Yang, H.-Y. K., Ruszkowski, M., & Zweibel, E. G. 2022, “Fermi and eROSITA bubbles as relics of the past activity of the Galaxy’s central black hole”, *Nat Astron*, 6, 584-591
- Zatsepin, G. T., & Kuz’min, V. A. 1966, “Upper Limit of the Spectrum of Cosmic Rays”, *JETP Letters*, 4, 78-80
- Zauderer, B. A., Berger, E., Soderberg, A. M. et al. 2011, “Birth of a relativistic outflow in the unusual γ -ray transient Swift J164449.3+573451”, *Nature*, 476, 425-428
- Zel’dovich, Ya. B., & Raizer, Yu. P. 1967, *Physics of Shock Waves and High-Temperature Hydrodynamic Phenomena*, Academic Press: New York
- Zhang, H.-S., Ponti, G., Carretti, E. et al. 2024, “A magnetized Galactic halo from inner Galaxy outflows”, *Nat Astron*, 8, <https://doi.org/10.1038/s41550-024-02362-0>
- Zirakashvili, V. N., Ptuskin, V. S., & Rogovaya, S. I. 2024, “Galactic origin of ultrahigh energy cosmic rays”, *PRD*, 110, 023016
- Zubovas, K., & Nayakshin, S. 2012, “Fermi bubbles in the Milky Way: the closest AGN feedback laboratory courtesy of Sgr A*?”, *MNRAS*, 424, 666-683